Three decades of Martian surface changes

Paul E. Geissler
U.S. Geological Survey, Flagstaff, Arizona, USA

Received 9 August 2004; revised 25 October 2004; accepted 11 November 2004; published 3 February 2005.

[1] The surface of Mars has changed dramatically during the three decades spanned by spacecraft exploration. Comparisons of Mars Global Surveyor images with Viking and Mariner 9 pictures suggest that more than one third of Mars' surface area has brightened or darkened by at least 10%. Such albedo changes could produce significant effects on solar heating and the global circulation of winds across the planet. All of the major changes took place in areas of moderate to high thermal inertia and rock abundance, consistent with burial of rocky surfaces by thin dust layers deposited during dust storms and subsequent exposure of the rocky surfaces by aeolian erosion. Several distinct mechanisms contribute to aeolian erosion on Mars. Prevailing winds dominate erosion at low latitudes, producing diffuse albedo boundaries and elongated wind streaks generally oriented in the direction of southern summer winds. Dust devils darken the mid to high latitudes from 45 to 70 degrees during the summer seasons, forming irregular albedo patterns consisting of dark linear tracks. Dust storms produce regional albedo variations with distinct but irregular margins. Dark sand dunes in southern high latitudes appear to be associated with regional darkening that displays diffuse albedo boundaries. No surface changes were observed to repeat regularly on an annual basis, but many of the changes took place in areas that alternate episodically between high- and low-albedo states as thin mantles of dust are deposited and later stripped off. Hence the face of Mars remains recognizable after a century of telescopic observations, in spite of the enormous extent of alteration that has taken place during the era of spacecraft exploration.

Citation: Geissler, P. E. (2005), Three decades of Martian surface changes, *J. Geophys. Res.*, *110*, E02001, doi:10.1029/2004JE002345.

1. Introduction

[2] One of the things that fascinates us most about Mars is its continually changing surface. Prior to the era of spacecraft exploration, seasonal variations and episodic changes were described by Earth-based observers starting with the early 19th century work of Flaugergues, and were widely believed to be caused by the growth and decay of Martian vegetation. Decades of telescopic photographic observations [e.g., *Slipher*, 1962, 1964] documented regional-scale variations, providing an important historical context into which to place the surface changes seen at close range by modern spacecraft. Many surface changes were observed between the Mariner and Viking missions and from one year of the Viking mission to another [*Sagan et al.*, 1972, 1973; *Veverka*, 1975, 1976; *Veverka et al.*, 1974, 1976, 1977; *Thomas and Veverka*, 1979]. Most of these changes were determined to have been produced by aeolian activity, through deposition of dust during local and global dust storms and subsequent darkening of the surface through erosion of the dust and transportation of sand. However, many questions about Martian surface changes remained unanswered. Because of the short time span of the earlier observations, it was difficult to determine which of the changes were seasonal variations and which were long-term alterations. In many cases, owing to the lack of high-resolution data, the exact causes of particular albedo changes were uncertain. The mechanisms and implications of Martian surface changes were not well understood.

[3] New data from the Mars Global Surveyor (MGS), Mars Odyssey and Mars Express missions are now available to help clarify the frequency, extent and causes of Martian surface changes. For this study we have used MGS Mars Orbiter Camera (MOC) daily global color images from the Wide-Angle Camera (WAC) to monitor the appearance of the Martian surface for the period from April 1999 to January 2003. These data enable us to estimate the present-day normal albedo of Mars under the clearest atmospheric conditions, distinguish albedo changes over the past two Martian years, and identify longer term surface changes from the Viking and Mariner 9 eras to the present. In addition, high-resolution images from the MOC Narrow Angle Camera (NAC) reveal the surface morphology of variable features in unprecedented detail, enabling us to examine the specific causes of Martian surface changes. Our objectives are (1) to map the surface changes that took place on Mars prior to the arrival of Mars Global Surveyor, (2) to document any seasonal

surface changes that may have taken place over the two Martian years of MGS observations, and (3) to investigate the causes of Martian surface changes by seeking correlations between variable features and surface characteristics such as elevation, geologic properties and predicted winds. From these observations we hope to discover what the surface changes can tell us about the interactions between the Martian surface and the atmosphere: Why do the variable features occur at the locations and seasons that they do? Are there regular seasonal changes such as an annual "wave of darkening" [*de Vaucouleurs*, 1954] that spreads from the spring hemisphere across the equator? What constraints do surface changes place on the strength of winds and the mobility of surface materials? What are the roles of dust devils and sand dunes in altering the Martian surface?

[4] This paper presents a global overview of Martian surface changes over the last three decades and explores the range of phenomena that can alter the albedo of the surface. In the next section we describe our procedures for constructing global mosaics from the color MOC WAC images and for producing a cloud-free summertime mosaic that can be compared to the best available Viking and Mariner data products. In section 3 we examine the MGS images for seasonal variations and surface changes that have taken place during the past two Martian years. Section 4 points out the major changes that have taken place between the end of the Viking Mission and the arrival of Mars Global Surveyor, and quantifies the areas affected in each case and the general setting of the variable feature in terms of elevation, slope, thermal inertia, rock abundance, and surface roughness. This section also presents a more detailed examination of five specific surface changes that apparently differ from one another in the manner and means by which they have altered. For these case studies, we consider the historical behavior of the regions, the presence of morphological features such as dust devil tracks, wind streaks, dunes, and bedrock, and the influence of regional winds predicted from theoretical models. The physical causes of surface changes and the new questions provoked by this research are discussed in section 5. In the final section, we draw conclusions from these observations about the extent and significance of surface changes over the last few decades and about the variety of mechanisms that alter the appearance of Mars over time.

2. Approach

2.1. MOC Global Color Mosaics

[5] In order to determine the present-day albedo of Mars and monitor any annual variations, we processed more than 2,000 MOC WAC global mapping swath color image pairs (a small fraction of the data available) that were acquired at resolutions between 3.2 and 8.2 km/pixel. These were assembled into 21 global mosaics showing the appearance of Mars at various seasons over a period of two Martian years. Each mosaic was produced by averaging approximately 100 color observations spanning several consecutive days. The individual images were first calibrated using procedures of the U.S. Geological Survey ISIS software, making use of preliminary Blue filter calibration coefficients derived by E. Eliason (personal communication, 2003). Next the images were navigated (appended with geometric information), assuming nadir pointing when necessary because of missing or unusable camera pointing information, and then reprojected to a common map projection with a nominal resolution of 10 pixels per degree. The data were next edited to eliminate images that could not be correctly calibrated because of missing information about gain changes during their exposures. Next the images were corrected for limb darkening using a wavelength-dependent Lunar-Lambert function, namely $R' = R/[(1 - L)\,\mu_0 + 2\,L\,\mu_0/(\mu_0 + \mu)]$ where R and R' are, respectively, the uncorrected and corrected radiance factors and μ_0 and μ are the cosines of the incidence and emission angles. The coefficients L of the Lunar-Lambert correction were derived empirically for the MOC Red and Blue filter images by creating test mosaics and minimizing the mismatch at the seams; the best fits were L = 0.6 for Blue and L = 0.25 for Red. The zero-phase-angle "hot spots" were deleted from the images along with data taken with incidence or emission angles greater than 84 degrees. Finally the images were averaged to produce mosaics, and the seams removed via the filtering procedure of *Soderblom et al.* [1978]. The green images were created by interpolating between the Red and Blue pictures. These procedures produced low-resolution mosaics of acceptable quality for the present purpose, but the results can be improved through better calibration and more sophisticated photometric corrections that would reduce the need for data redundancy. Even with the extensive averaging of images that we employed, there remain artifacts in these mosaics in the form of faint (<2.6%) streaks in the orbit-track directions.

2.2. Construction of MOC Frost- and Cloud-Free Mosaic

[6] Each of the individual mosaics described above includes frosts, clouds and hazes that obscure different portions of the surface at various times of the Martian year. Like the MOC Geodesy Campaign mosaic [*Caplinger*, 2002], they are snapshots of Mars at particular seasons, and the wintertime pole is generally in darkness. Construction of a cloud-free, summertime mosaic was achieved by combining the darkest pixels of all the individual mosaics acquired at different seasons into a single color picture. This was done separately for the Red and Blue filter data, and a synthetic green image was again derived by interpolating the resulting Red and Blue mosaics. Seasonal differences in overall brightness from one mosaic to another due to the changing distance of Mars from the Sun were first removed by normalizing the brightness of all the Red and Blue mosaics at low latitudes unaffected by the polar hoods. Because of minor genuine surface changes that were apparent after the global dust storm of 2001 (section 3), only data from the first 14 mosaics (up to phase E05) were used in the production of the cloud-free mosaic.

2.3. Viking Color Mosaic Data and Processing and Comparison to MGS

[7] In section 4 we will compare the MOC cloud-free mosaic to the U.S. Geological Survey Viking color Mars

Digital Image Model (MDIM) produced by *McEwen et al.* [1994]. Here we briefly review the steps that went into creating the Viking mosaic in order to establish that the comparison between these two products can be safely made. McEwen et al. began by making mosaics of images from 57 individual Viking orbits using data with phase angles ranging from 13 to 85 degrees. These single-orbit apoapsis mosaics were corrected for limb-darkening using a Minnaert function and the best quality images were chosen to represent clear atmospheric conditions and held constant while the others were adjusted in brightness to match. Frost-free regions that were unusually bright in the Violet filter images were assumed to be shrouded by atmospheric haze, and a conservative estimate of the haze brightness was subtracted from both the Red and Violet filter images. This procedure improved the consistency of the Red filter albedo maps, but the Violet filter values are somewhat less reliable. The images were next mosaicked by placing the best quality images (generally those taken at the lowest phase angles) on top, and the seams removed by the same filtering procedure as used for the MOC mosaics. Finally, the mosaic was sharpened by adding high-frequency components derived from the Red filter image, and the green mosaic was interpolated from the Red and Violet filter data.

[8] For quantitative purposes, only the Red filter data from both Viking and MGS were used to measure albedo changes by subtracting the coregistered Viking Red MDIM from the MOC Red mosaic. We first applied a linear contrast stretch to the Viking data to match the brightness of the MOC image, computed by a least squares fit between the data sets, in order to compensate for differences due to photometric conditions and normalizations, calibration, spectral bandpass and processing techniques. A plot of the MOC Red filter radiance versus the corresponding Viking Red radiance helps constrain the uncertainty in this procedure; most of the pixels from unchanged regions lie along a linear trend with a dispersion (width) equal to ~5% of the variability. The principal remaining source of error in this comparison is the variation in phase angle between the two data sets. This is particularly apparent in the high southern latitudes, where topographic relief is enhanced in the Viking mosaic and albedo variations are subdued. In places where there was ambiguity over whether surface changes were real, we consulted original Viking images and single-orbit mosaics that were acquired at the lowest available phase angles in order to verify each case. An independent estimate of albedo is provided by the broadband solar albedo images acquired by the Thermal Emission Spectrometer (TES) on MGS and similar images produced by the Viking Infrared Thermal Mapper (IRTM). Although these data are of lower resolution, cover latitudes only between 60°S and 60°N, and have their own issues concerning seasonal differences and the presence of clouds and hazes, they provide a useful consistency check on the inferences drawn from the imaging data.

[9] The surface areas affected by each change were computed by counting pixels in equal-area map projections. For each surface change we estimated the total area that had visibly altered and also the area that had altered by at least 10% of the mean planetary albedo (twice the uncertainty estimated above). Where these values differ greatly from the estimates derived from the TES and IRTM solar albedo images, we list the areas estimated from both data sets.

3. MGS to MGS Variations (1999–2003)

[10] Figure 1 shows a series of snapshots of Mars as it appeared over the first two years of MGS observations. A color animation of these observations can be viewed at http://astrogeology.usgs.gov/Projects/MarsChanges. Many seasonal variations can be seen that repeat from one Martian year to the next. All of the observed seasonal variations can be ascribed to atmospheric effects or surface frost. The growth and retreat of the polar caps, the appearance and disappearance of polar hoods, and the occurrence of equatorial clouds atop the volcanoes were much as predicted from decades of Earth-based observations [*Capen*, 1976] (J. Beish, The Master Calendar of Events on Mars, 2004; available at http://www.tnni.net/~dustymars/predict.htm). The great basins of Hellas and Argyre brightened during southern hemisphere winter due to deposition of surface frosts. Surface contrast was reduced during periods of high atmospheric dust opacity, particularly during the global dust storms of June to October 2001 (see Figure 1 phase E09).

[11] No periodic changes in albedo patterns were detected. The boundaries of bright and dark regions did not appear to shift on an annual basis. However, a number of episodic changes took place during the global dust storm of 2001. Most of these changes were relatively subtle, including brightening (presumably due to dust deposition) along the west margin of Syrtis Major (near 18°N, 300°W), portions of Nilosyrtis (40°N, 280°W), northeast of Hellas (27°S, 270°W), and to the northwest of Elysium (32°N, 235°W). Other areas darkened during the dust storm, perhaps through removal of dust by unusually strong winds: darkening occurred near the boundary between Hesperia and Elysium (7°S, 235°W), at Sinai (16°S, 90°W), and in the eastern part of Aonius Sinus (30°S, 110°W). The brightening of Syrtis and darkening at Sinai and Aonius, although minor in extent, are important because the changes began to restore these areas to their former Viking-era appearance, reversing the surface changes that took place between the Viking and MGS observations (section 4). While they are not "seasonal" changes per se, they are among many areas of Mars that appear to alternate between dust-covered and dust-free states repeatedly over timescales of decades.

[12] The two Martian years of MGS observations highlight some of the hazards to be avoided when looking for long term surface changes. In general, albedo patterns do not alter on an annual basis but the contrast changes dramatically with the season. The apparent surface albedos in dark areas such as Syrtis and Acidalia depend strongly on atmospheric opacity. These regions often appear fainter during the annual dust storm season in southern spring and summer. Small-scale albedo patterns are easily obscured by dust storms, clouds and hazes that can be misinterpreted as seasonal surface changes. The MOC imaging results are consistent with the conclusions of *Pleskot and Miner* [1981], who found no seasonal variations in surface albedo over the Martian year 1976–1978, which included the global dust storms of 1977.

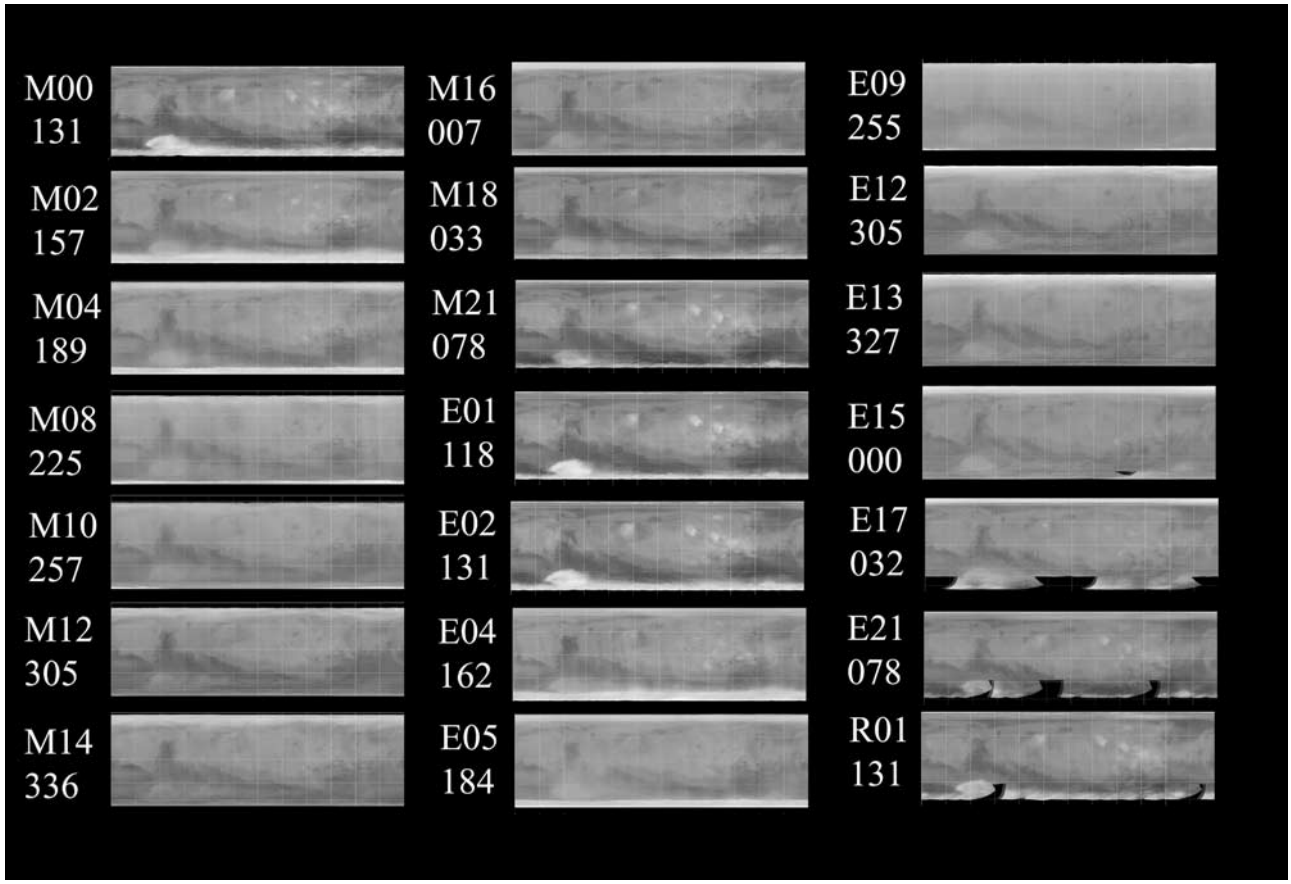

Figure 1. Time series of MGS global monitoring images. This montage of red filter MOC WAC mosaics shows the appearance of Mars at various times during each of two Martian years from 4/1999 to 1/2003. The mosaics are shown in equal-area cylindrical map projections and are labeled with the MGS mission phase and the solar longitude (Ls). Seasonal phenomena that can be seen in these snapshots include the annual appearance of polar hoods and surface frosts, brightening within the great basins of Hellas and Argyre, and the occurrence of equatorial clouds adjacent to the volcanoes of Tharsis and Elysium. The global dust storm of 2001 obscured surface albedo contrast (especially during phase E09) and produced many minor surface changes.

These authors suggested that the reported ''wave of darkening'' is the result of contrast sharpening with increasing atmospheric clarity.

4. Viking to MGS Changes

[13] Much greater surface changes were seen over the 10 Martian year interval between Viking and MGS. Figures 2a–2c show a comparison between the Viking color MDIM of *McEwen et al.* [1994], constructed of images taken from 1976 to 1980, and the cloud-free MOC mosaic made up of images acquired from 1999 to 2001. An animation that blinks between these two pictures can be viewed at http://astrogeology.usgs.gov/Projects/MarsChanges. Several significant changes are evident from this comparison. In general, the high-latitude regions darkened during this period whereas the equatorial regions brightened, consistent with the findings of *Bell et al.* [1999] from Hubble Space Telescope (HST) observations that were compared to Viking IRTM measurements. A small bright band formed around the north pole of Mars, and the large dark band surrounding it shifted toward the eastern hemisphere and expanded along its southern margin. A large dark ring formed around the south pole. Many of the classical albedo features along the equator shifted or changed shape, including Syrtis, Alcyonius, Hyblaeus, Propontis, Cerberus and Acidalia (all of these changes are described in detail below). Such changes along sharp albedo boundaries are much easier to spot than the more subtle changes in the albedos of broad regions or those with diffuse albedo boundaries.

[14] The surface changes are quantified in Figure 3, which displays the difference between the present-day appearance of Mars and its appearance during 1976–1980 after subtracting the Viking era albedo from the MGS measurements. (These difference images are preferable to calculating ratios because subtraction avoids the instability introduced by dividing small quantities in low-albedo regions). In general, the visible imaging results (Figure 3, top) agree with estimates derived from the broadband solar albedo channels of the thermal imaging instruments (Figure 3, bottom), but there are several differences between the data sets that may be explained by differences in bandpass, season or phase angle. In particular, the

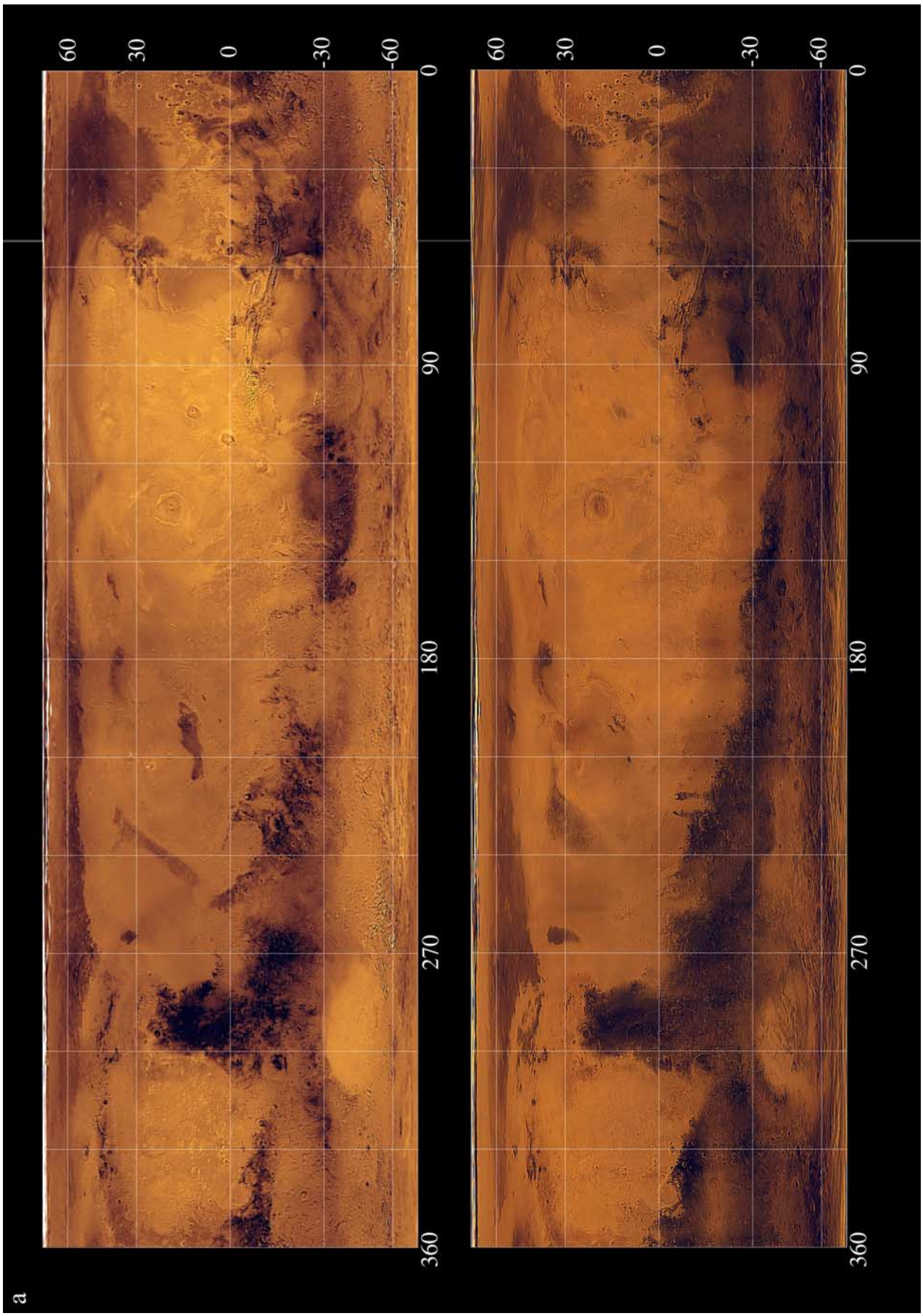

Figure 2

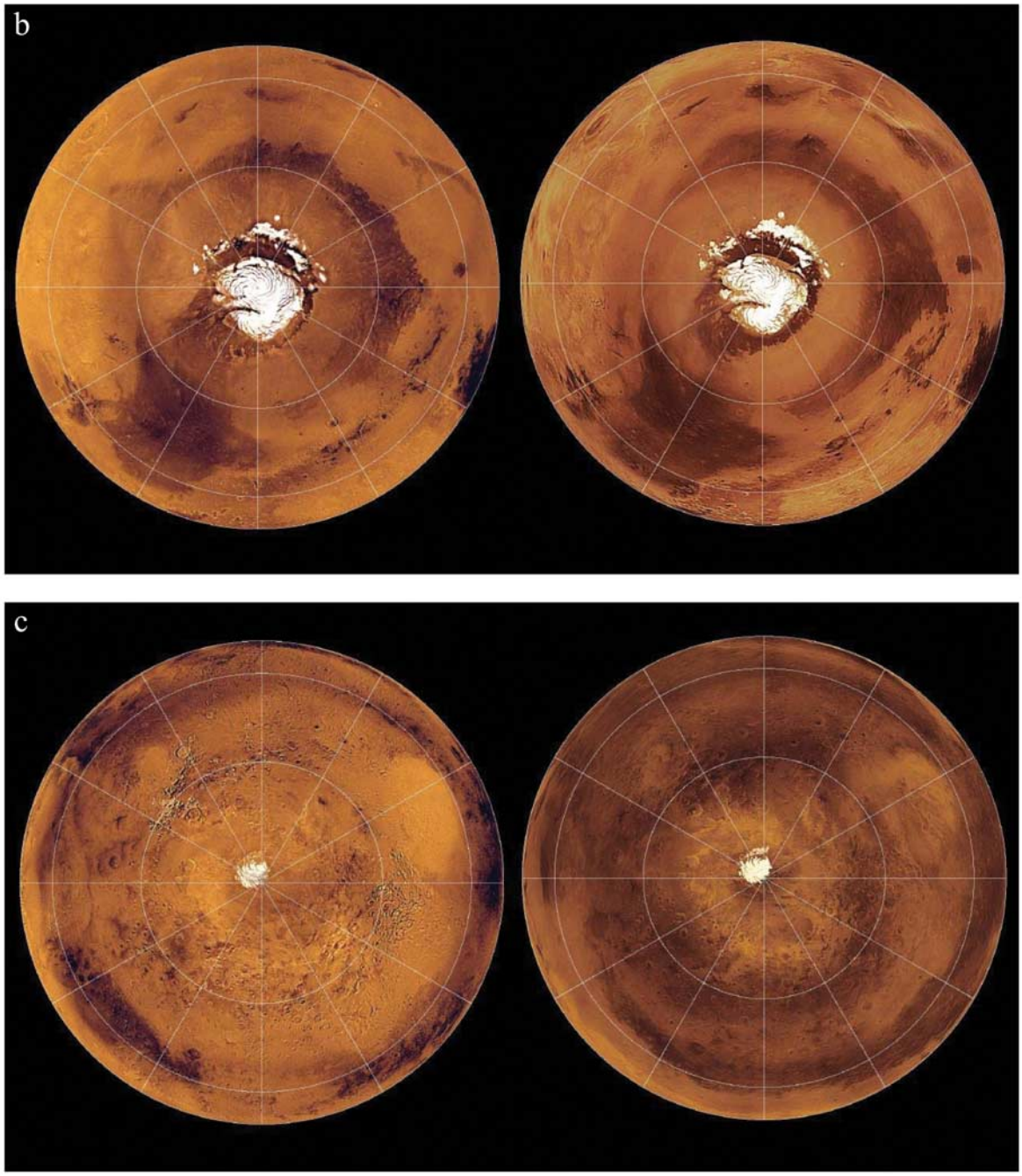

Figure 2. (continued)

imaging results suggest brightening in Amazonis and darkening around the Valles Marineris that are not apparent in the TES - IRTM albedos. The visible imaging albedos are derived from the Red filter data as described in section 2; the bandpass of the Viking visual imaging subsystem (VIS) Red filter was from 550 to 700 nm, whereas the MOC Red filter spans a narrower range from 600 to 630 nm. Both of these are much narrower than

Figure 2. Comparison of Viking and MGS global mosaics of Mars. Shown here are side-by-side comparisons of the color digital image mosaic assembled by *McEwen et al.* [1994] from Viking images acquired during the period 1976–1980, and the cloud-free mosaic of MGS images from 1999 to 2001. All of the large-scale surface changes discussed in this paper are obvious in these renditions. Note in particular the new dark ring centered on latitude 60°S that is apparent in Figure 2c. (a) (top) Viking color DIM versus (bottom) MGS cloud-free mosaic in equal-area cylindrical map projections. (b) (left) Viking and (right) MGS views of the northern hemisphere of Mars in polar orthographic map projections. (c) (left) Viking and (right) MGS views of the southern hemisphere of Mars in polar orthographic map projections.

the albedo channels of the thermal instruments, which were sensitive to wavelengths from 300 to 2900 nm. The MGS TES albedo is from *Christensen et al.* [2001, Plate 14]. The northern hemisphere TES measurements were made during late northern summer at solar longitudes (Ls) 100–150, prior to mission phase M02. The southern hemisphere observations were made in early southern summer at Ls 270–330 during phases M10 to M13. The Viking IRTM albedo is from *Pleskot and Miner* [1981] and *Kieffer et al.* [1982] with refinements by *Christensen* [1988]. The northern hemisphere IRTM measurements were collected at Ls from 337 to 186, and the southern hemisphere observations Ls ranged from 120 to 360.

[15] For this paper we will focus attention on the large scale surface changes that can be seen in both the imaging and thermal instrument albedo measurements. The locations of these major changes are shown in Figure 4, which also shows the general relationships of the surface changes to global topography and thermal inertia from MGS measurements. Following are descriptions of each of these surface changes in the order in which they are numbered in Figure 4. In addition to the albedos and areas affected by each change, we describe the topographic setting of each site and give information about the physical properties of the surface derived from thermal measurements and laser altimetry. These independently measured surface properties are from several sources and were acquired at various different times. We quote TES values for broadband albedo [*Christensen et al.*, 2001] and thermal inertia [*Mellon et al.*, 2002]. Rock abundances are as derived from Viking IRTM analyses [*Christensen*, 1986]. MGS Mars Orbiter Laser Altimeter (MOLA) data were used to obtain elevations [*Smith et al.*, 2003] and surface roughness estimates based on laser pulse width measurements [*Neumann et al.*, 2003; *Deal et al.*, 2003]. Table 1 provides a summary of typical surface properties at each of the major surface changes along with measurements of neighboring areas that remained unchanged.

4.1. Syrtis Major

[16] Figure 3 shows that the northwest margin of this classical albedo feature darkened during the interval between Viking and MGS. The darkening took place in the vicinity of 20°N, 290°W. The southwest margin of Syrtis brightened during this period. The interior of Syrtis Major appears to have brightened but, as pointed out earlier, this appearance could be caused by atmospheric effects unrelated to surface changes [e.g., *Akabane et al.*, 1990]. The area along the edges of Syrtis that can be shown to have visibly altered totals 428,000 km^2, of which 62,000 km^2 darkened by more than 10%. The TES broadband albedo in the darkened zone ranges from 0.13 to 0.18, to be compared to TES albedos elsewhere in the vicinity that range from 0.10 in the dark center of Syrtis up to 0.25 in bright, dust-covered regions. The changes took place on the sloping margin of a broad plateau (Syrtis Major Planum), at elevations ranging from 0 to 1000 m above datum. The region is locally high in both TES thermal inertia (200–400 J m^{-2} K^{-1} s$^{-1/2}$, henceforth abbreviated as "mks units") and IRTM rock abundance (10% to 20%), even though the rock abundance was calculated from Viking data when the region was in its bright (presumably dust-covered) state. The western margin of Syrtis brightened again after the global dust storm of 2001, partly restoring the region to its former Viking era appearance. Frequent changes in the width of Syrtis Major have long been noted by Earth-based telescopic observers [e.g., *Capen*, 1976], and can perhaps be explained by cyclic deposition and erosion in this zone.

[17] In addition to the changes to the north and west of Syrtis, minor changes took place to the south and east near the Lybia Montes. Variations in this area were recognized at the time of the Phobos 2 mission in 1989 [e.g., *Erard et al.*, 1991].

4.2. Nilosyrtis and Alcyonius

[18] Several major changes occurred to the north of Syrtis. Most obvious is the enlargement of a broad, dark band that covers latitudes from 50°N to 60°N and longitudes from 180°W to 300°W, which is best seen in the north polar projection of Figure 2b. This band includes the classical albedo features Nilosyrtis, Utopia, and Cebrenia. The albedo boundary that separates the dark band from brighter regions shifted southward, particularly at Nilosyrtis (43°N, 275°W) where TES and IRTM data indicate that the surface albedo dropped by up to 50%. Figure 5 shows an overview of the changes that took place in Casius Quadrangle in the period between the Viking and MGS observations. The northern low-albedo region (Nilosyrtis) greatly enlarged during this interval, and the albedo boundaries between bright and dark terrain are sharply defined but irregular in plan. An area of 1.1 million km^2 was visibly altered, and 688,000 km^2 darkened by more than 10%. The TES albedo of the darkened zone ranges from 0.11 to 0.16 with an average of 0.12. The changes took place on the slopes of a shallow depression (Utopia Planitia) in the plains of Vastitas Borealis, at elevations from −4950 m to −3500 m. The TES thermal inertia in the changed area is moderate to high, ranging from 220 to 310 mks units with an average of 275–285. The Viking IRTM rock abundance is also high, from 16% to 25%. The MOLA roughness of the region is low to moderate.

[19] South of this band, a much smaller area of 161,000 km^2 darkened when the classical albedo feature Alcyonius (sometimes called Thoth), at 30°N, 265°W, enlarged. Unlike Nilosyrtis, the albedo along the southern boundary of Alcyonius transitions gradually from dark to bright without the complexity seen farther north. The TES albedo in the darkened zone is 0.13 to 0.14, a reduction of 0.07 to 0.09 from its Viking appearance. An area of at least 117,000 km^2 darkened by 0.02 or more. Like many low-latitude surface changes, the darkening of Alcyonius took place on a sloping surface with relatively high thermal inertia and rock abundance, suggesting that a thin veneer of dust was stripped off a bedrock surface during periods of high winds. Elevations in this region range from −4500 m to −3500 m. The TES thermal inertia varies from 230 to 290 mks units, averaging 245 to 265, and the IRTM rock abundances average 10% to 15%.

[20] Historical records indicate that the growth of Nilosyrtis and Alcyonius began before the arrival of Viking and is gradually restoring the region to its appearance of 50 years ago. Telescopic images show

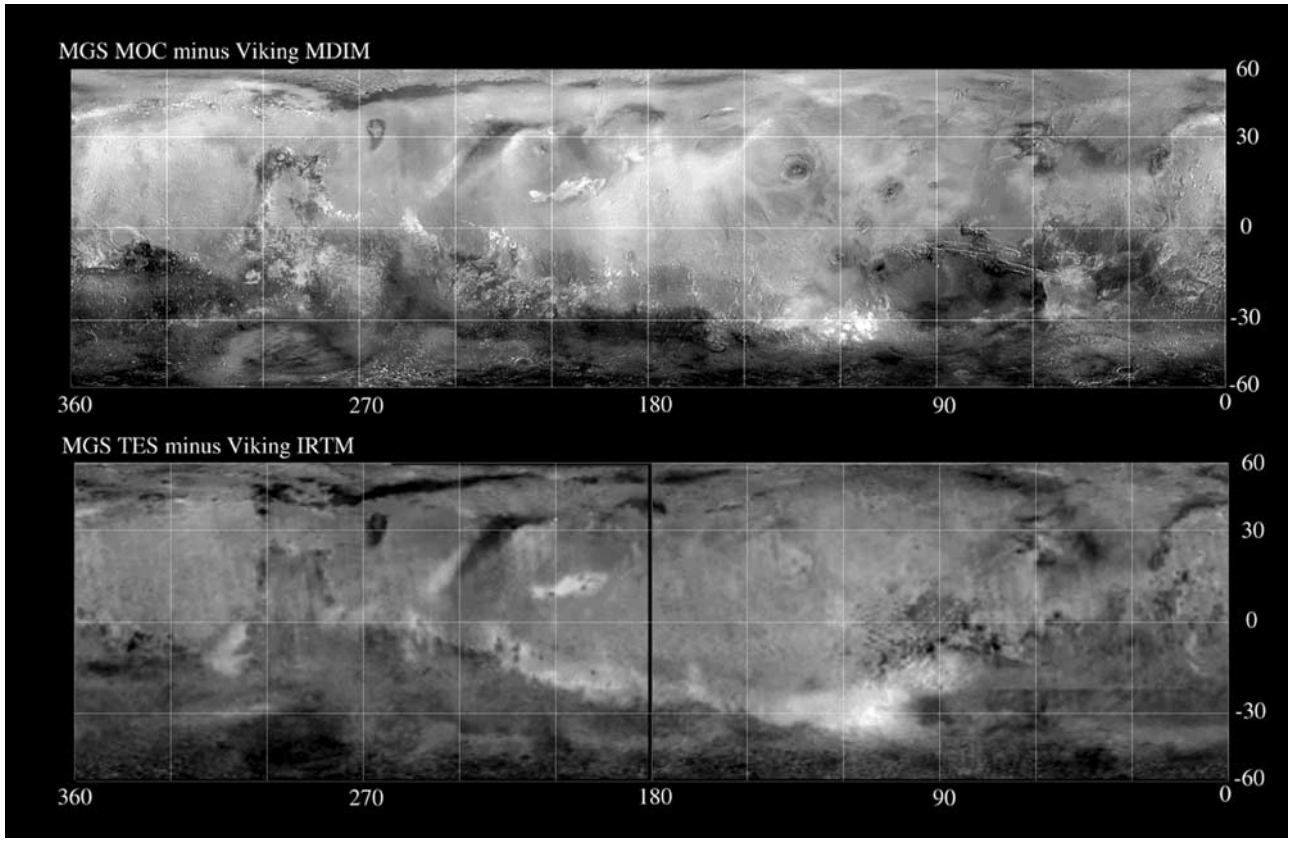

Figure 3. Differences between Viking and MGS albedos of Mars. These images map the albedo changes that took place between Viking and MGS as seen by two types of sensors. The top image shows albedo changes computed by subtracting the Viking red filter image mosaic of *McEwen et al.* [1994] from the cloud-free red filter mosaic from MGS MOC. The image is scaled so that black tones represent a decrease in albedo of −0.06 (I/F) and white represents an increase of +0.03. The bottom image shows a similar result, produced by subtracting the Viking IRTM broadband albedo from the MGS TES broadband albedo, stretched to portray a range of albedo changes from −0.09 to +0.09. The images are presented in equal-area map projections from 60°S to 60°N, the limits of reliable IRTM coverage. Both of the data products indicate darkening at higher latitudes, particularly in the southern hemisphere, and brightening at tropical latitudes.

extensive areas north and east of Syrtis that were dark in 1954 [*Slipher*, 1962, Plate IX] but had brightened by 1969 [*Martin et al.*, 1992]. Alcyonius was completely buried at the time Mariner 9 observed the region in 1972, but had already begun to emerge by the arrival of Viking. Both Alcyonius and Nilosyrtis enlarged over the course of the Viking Mission, undergoing changes that affected tens of thousands of square km from 1978 to 1980 (Figure 6).

[21] The bedrock in this region is the Hesperian Vastitas Borealis Formation of undetermined origin [*Greeley and Guest*, 1987]. Superposed on these rocks are many features shaped by periglacial processes including irregular scalloped depressions formed by sapping or sublimation and vast areas of polygonally patterned ground that feature small (50–100 m diameter), regular polygons believed to be caused by the presence of ice (ice wedges) or liquid water (mud cracks) in the sediments [*Mellon*, 1997; *Seibert and Kargel*, 2001]. These polygons are quite distinct in the dark areas but are faint or absent in bright areas, as if obscured by thin mantles of dust. The transition between polygonally patterned ground and adjacent smooth, brighter surfaces is quite gradual (see, e.g., MOC NAC images E0401425, E2301288).

[22] High-resolution MOC NAC images of the recently darkened areas in Nilosyrtis present strong evidence for erosion by dust devils. Figure 7 shows a close-up of a newly darkened zone at 54.28°N, 292.69°W. At this resolution (6.6 m/pixel), the darkest patches can be seen to be criss-crossed with filamentary linear streaks that are diagnostic of dust devil tracks [*Grant and Schultz*, 1987; *Edgett and Malin*, 2000; *Malin and Edgett*, 2001; *Balme et al.*, 2003]. Dust devil tracks are absent from the nearby bright regions and are also largely absent from lower-latitude dark patches such as Alcyonius. The tracks appear to form seasonally, commonly appearing during northern spring and summer. A survey of MOC NAC images from mission phases AB1 to E06 identified dust devil tracks in 107 NAC images. Definitive nondetections were made in another 180 NAC images. The distribution of detections (black) and non-detections (white) for all these cases is shown in Figure 8. The dust devil tracks are strongly zoned during all seasons, confined to latitudes ~45°N to ~65°N. In areas such as Alcyonius that darkened outside of this latitude

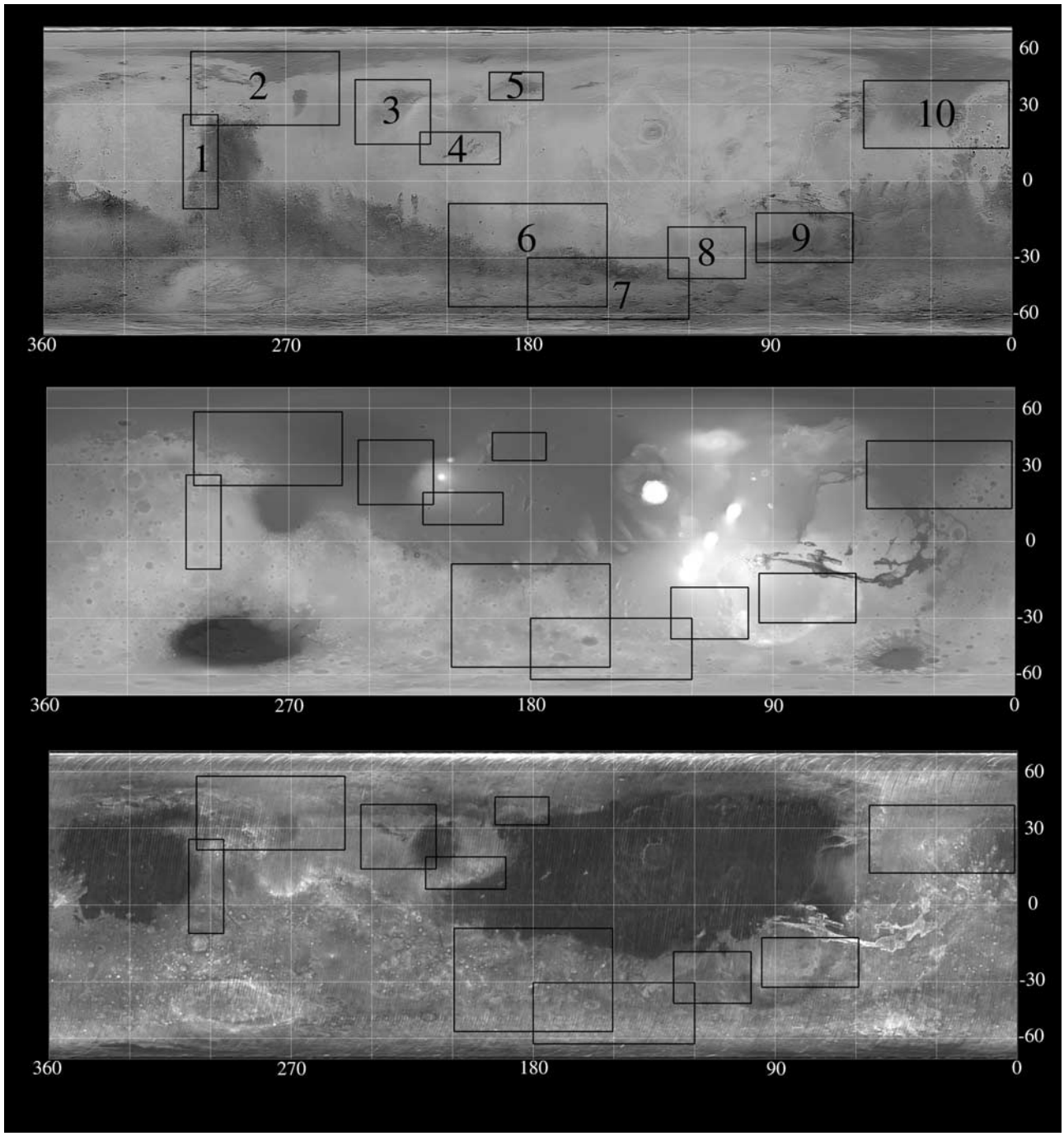

Figure 4. Locations of large-scale surface changes. Boxes outlining the major surface changes described in the text are overlain on (top) an MGS MOC red filter mosaic, (middle) a gray scale rendition of MOLA topography, and (bottom) a map of thermal inertia from MGS TES. Note that all of the major surface changes took place in areas of moderate to high thermal inertia. The individual albedo features discussed in section 4 are as follows: 1, Syrtis Major; 2, Nilosyrtis and Alcyonius; 3, Hyblaeus; 4, Cerberus; 5, Propontis; 6, Southern Tropical Dark Band (Mare Cimmerium-Mare Sirenum); 7, Southern High-Latitude Band (Mare Chronium-Mare Australis) at Phaethontis Quadrangle; 8, Aonius Sinus; 9, Solis Lacus; 10, Acidalia.

band, dust devil tracks are absent and the surface is pervaded instead by wind streaks indicative of prevailing winds.

[23] Northern spring and summer winds are light (<5 m/s) throughout the region that underwent surface changes, according to the predictions of the Geophysical Fluid Dynamics Laboratory Mars Global Circulation Model (GFDL MGCM) [*Wilson and Hamilton*, 1996; *Fenton*, 2003]. Southern spring and summer winds are predicted to be lighter in the northern portion of the region (the area

Table 1. Physical Characteristics of the Sites of Major Surface Changes and Adjacent, Unchanged Regions, Determined From 0.7° × 0.7° Areas Centered on the Listed Map Coordinates[a]

Name	Latitude	Longitude	Visible Albedo Change MOC-MDIM	σ	Solar Albedo Change TES-IRTM	σ	Elevation, m	σ	Slope, m/deg	σ	TES Thermal Inertia, J m^{-2} K^{-1} s$^{-1/2}$	σ	IRTM Rock Abundance, %	σ	TES Albedo	σ
Syrtis darkened	18.7	299.5	−0.017	0.004	−0.027	0.001	386	90	683	458	292	28	14.8	1.7	0.158	0.003
Syrtis unchanged	14.0	303.8	0.011	0.002	0.007	0.003	851	28	230	146	142	15	8.0	0.0	0.238	0.001
Nilosyrtis darkened	42.6	271.1	−0.051	0.001	−0.107	0.002	−4148	51	219	169	272	7	12.0	3.2	0.132	0.004
Nilosyrtis unchanged	38.7	268.4	0.003	0.001	−0.032	0.001	−4201	16	101	48	261	9	17.9	3.7	0.234	0.000
Alcyonius darkened	27.2	265.3	−0.022	0.001	−0.077	0.003	−3720	7	53	28	263	10	17.3	3.6	0.171	0.004
Alcyonius unchanged	26.2	268.9	0.007	0.001	−0.035	0.004	−3517	29	227	187	210	43	10.0	0.0	0.242	0.004
Hyblaeus brightened	16.0	243.8	0.019	0.003	0.031	0.002	−3102	103	689	417	265	12	13.6	3.5	0.230	0.002
Hyblaeus unchanged	22.7	243.6	0.001	0.001	−0.027	0.002	−3942	31	173	97	271	13	10.0	2.9	0.220	0.000
Hyblaeus darkened	33.1	225.6	−0.044	0.001	−0.092	0.001	−4255	25	143	78	233	10	11.1	1.4	0.173	0.001
Cerberus brightened	11.3	215.9	0.046	0.009	0.026	0.007	−1967	62	378	153	254	7	5.0	0.0	0.244	0.002
Cerberus unchanged	13.5	215.6	0.016	0.001	−0.008	0.001	−884	142	691	300	211	15	4.3	2.5	0.260	0.002
Propontis darkened	38.4	175.9	−0.024	0.002	−0.067	0.009	−3997	21	109	72	199	13	15.0	3.5	0.165	0.008
Propontis unchanged	36.6	172.3	0.009	0.002	−0.028	0.002	−3903	41	316	201	96	14	10.7	0.8	0.247	0.002
Sirenum darkened	−30.7	163.6	−0.058	0.002	−0.040	0.001	2230	53	382	317	211	7	5.0	1.8	0.133	0.002
Sirenum unchanged	−31.5	158.8	−0.004	0.004	−0.018	0.002	1931	41	564	746	251	21	5.1	0.3	0.125	0.003
Phaethontis darkened	−52.2	151.9	−0.074	0.001	−0.101	0.004	1435	32	218	98	284	30	NR	NR	0.140	0.000
Aonis brightened	−32.1	117.7	0.060	0.004	0.074	0.002	3588	122	995	940	194	14	8.1	0.3	0.237	0.002
Aonis unchanged	−23.7	117.1	−0.005	0.002	0.055	0.003	4608	36	216	86	169	8	5.1	0.3	0.238	0.001
Solis darkened	−26.4	87.3	−0.057	0.002	−0.025	0.001	2937	30	143	79	340	13	9.1	1.8	0.132	0.003
Solis unchanged	−30.3	76.3	−0.008	0.005	−0.014	0.003	4453	190	977	357	173	12	9.1	0.7	0.152	0.002
Acidalia darkened	−22.7	39.4	−0.047	0.001	−0.052	0.001	−3868	7	68	34	358	10	14.6	1.8	0.149	0.002
Acidalia unchanged	14.9	29.4	0.002	0.004	−0.007	0.001	−3406	233	1090	811	278	16	8.9	1.0	0.248	0.003
Acidalia brightened	35.5	8.7	0.023	0.003	0.009	0.002	−3256	59	433	429	207	14	12.3	0.7	0.247	0.002

[a]The tabulated uncertainties (σ) represent one standard deviation. NR, not reported.

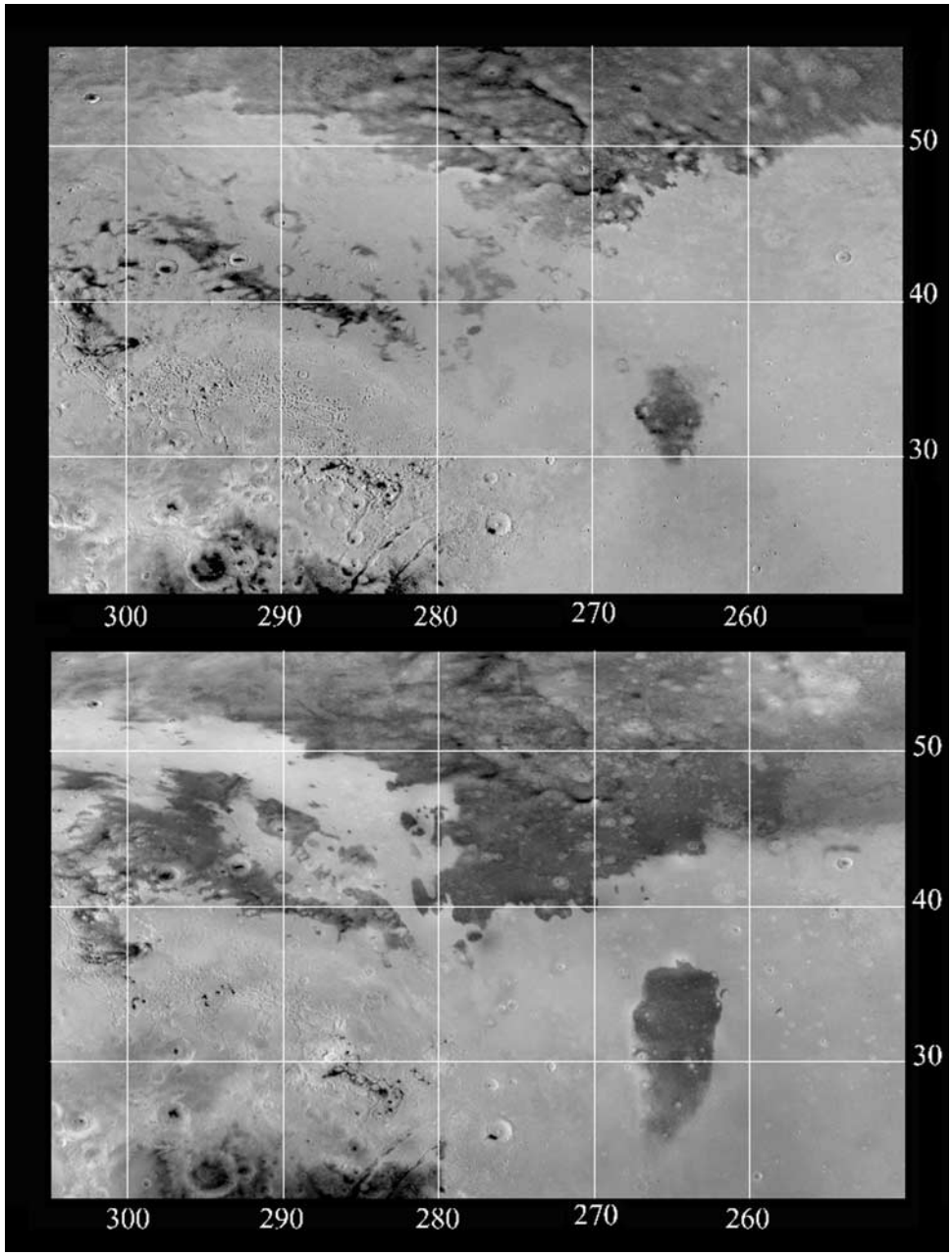

Figure 5. Surface changes at Nilosyrtis and Alcyonius. Nilosyrtis is the name given to the dark terrain in the northern part of this region. Alcyonius is the isolated dark patch to the southeast of Nilosyrtis. Both of these low-albedo zones enlarged between the time of (top) the Viking images and (bottom) the MGS observations. Note the complex and sharply defined albedo boundaries dividing bright and dark terrain. These images span an east-west distance of 2440 km at 40°N latitude. The MGS mosaic shown is from *Caplinger* [2002].

where dust devil tracks are common) than in the south (where no tracks are seen).

4.3. Hyblaeus

[24] This classical dark albedo feature (also known as Aetheria) brightened and a new dark patch appeared to the east, bordering the volcano Elysium. These changes took place on the sloping surface between Utopia and Elysium, at elevations ranging from −4400 m to −2000 m. The northwestern slopes of Elysium also brightened during this interval between Viking and MGS. The changes were centered at 25°N, 240°W but affected an area of about 1.2 million km^2. Approximately 304,000 km^2 darkened by more than 10%, while at least 160,000 km^2 brightened by this amount. The TES albedo in the newly brightened area is 0.22 to 0.24, compared to 0.17 to 0.19 in the dark patches. The thermal inertia ranges from 180 to 400, but averages 225–250 mks units. The Viking rock abundance prior to the change was slightly greater (10%–15%) in areas that were dark at the time of the observations than in

bright areas (8%–9%). Mariner 6 and 7 images show the Hyblaeus albedo feature absent in 1969, similar to its appearance in the MGS era [*Edmonds and Robinson*, 2003].

4.4. Cerberus

[25] The brightening at Cerberus (10°N, 205°W) provides an opportunity to examine both the nature of dust deposition and the earliest stages of erosion. Figure 9 shows an overview of the changes in the Cerberus region. Several previous studies have pointed out that this classical low-albedo feature disappeared sometime between the end of the Viking Mission and the opposition of 1995 [*Lee et al.*, 1996; *Bell et al.*, 1999; *Erard*, 2000], perhaps before late 1990 [*Moersch et al.*, 1997]. The low-albedo materials, which extended across a region nearly 1400 km long and 250 km wide, are presently completely buried except for a few dark patches in the eastern and western reaches. The (probable) new dust deposits mantled an area of nearly 390,000 km^2, of which 245,000 km^2 brightened more than 10%. The TES albedo increased from 0.15–0.18 in the dark patches up to 0.23–0.25 in the newly brightened zone. The changes took place on the southern slopes of the Elysium rise, at elevations from −2500 m to −1800 m. TES measurements indicate that the zone occupies a bench of locally high thermal inertia averaging 250–290 mks units with a range of 220–350. Viking IRTM rock abundances were also locally high, averaging 9% to 11%. The MOLA roughness in this area is average except for some relatively rough regions in the east, near Cerberus Fossae.

[26] Cerberus appeared dark and apparently unchanged from 1907 to 1954 [*Slipher*, 1962, Plate XXXV] but darkened and enlarged between Mariner 9 in 1972 and the arrival of Viking in 1978 [*Chaikin et al.*, 1981]. The darkening and changes in direction of wind streaks were interpreted by Chaikin et al. to be caused by the removal of bright dust. The region remained dark in Viking Orbiter 1 observations acquired in 1980 (orbit 323S). Pic du Midi telescopic observations [*Lecacheux et al.*, 1991] show Cerberus already partially obscured in 1988, with further changes taking place in 1995 [*Erard*, 2000]. Possibly the feature was buried during the global dust storm of 1982.

[27] Cerberus lies on the margin of early Amazonian lava flows from Elysium but is also the site of some of the youngest lava flows, channels and alluvial deposits on Mars [*Plescia*, 1990, 2003; *Burr et al.*, 2002a, 2002b; *Berman and Hartmann*, 2002]. The classical albedo feature is cut by two northwest-trending linear troughs, called the Cerberus Fossae, believed to be volcanic fissures that are the source of both the lavas and the floodwaters.

[28] High-resolution images show several morphological indications that the new dust deposit covering the region is quite thin. Dust devil tracks, produced by removal of a bright layer exposing a darker substrate, appear sporadically in northern hemisphere summer (e.g., MOC NAC images M0001273, M0002500, E1400795, E1601013, E1601635). Many small craters that are located in the bright dust-covered regions have dark floors, perhaps cleaned of dust by turbulent winds (MOC NAC images M0002500, M0201973, M0204698, M0400964, M0402835, M1300846, M1301354, E1600925; see also Figure 10). These imaging observations are consistent with the interpretation of ground-based thermal data [*Moersch*, 1998] that a layer of dust only 2 to 4 mm thick currently covers the Cerberus region.

[29] Erosion at Cerberus is dominated by prevailing northeasterly winds, as shown by the numerous bright and dark streaks that extend hundreds of km toward the southwest from topographic irregularities such as knobs, impact craters and the Cerberus Fossae troughs. Northeasterly winds (i.e., from the northeast) are predicted by the GFDL MGCM to reach average strengths of up to 20 m/s during southern spring and summer. Figure 10 shows the early stages of erosion in an area near 13.96°N, 199.51°W that is still mostly covered by dust. Incipient dark streaks are initiated at topographic obstacles such as craters and knobs, while the interiors of the larger craters have been filled with dust that has been organized into dune-like ripples with wavelengths on the order of a few tens of meters. Elsewhere in Cerberus, where erosion has progressed more fully, these dust-filled craters lie windward of bright streaks representing the last of the dust to be removed from the region. While dominated by prevailing winds, erosion is also contributed to by dust devils (as noted above) and sand dunes locally appear to play a role as well. Several dark streaks arise from "splotch craters", impact craters that are occupied by dark patches on their downwind sides. Only one of these dark patches has so far been imaged by MOC NAC; giant dark dunes with wavelengths of several hundred meters are seen in image E1701373, inside the crater at 9.5°N, 210°W. This crater heads a broad, diffuse dark patch that trails west-southwest for more than 100 km from the crater rim. This zone of erosion could be produced by winds interacting with the crater's topography, but it is possible instead that sand escaping from the dark dunes acts to darken the downwind surface. The potential mechanisms by which sand dunes might darken adjacent terrain are discussed in section 5.

4.5. Propontis

[30] An area of about 190,000 km^2 darkened in Arcadia Planitia near 37°N, 185°W. This change took place within a low, flat plain at elevations from −4000 m to −3800 m. The low relief of this region demonstrates that erosion is not restricted to sloping surfaces. The TES albedo of the region is highly variable, ranging from 0.13 to 0.19. Imaging data suggest that only 58,000 km^2 darkened more than 10%, but the broadband albedo estimates from TES and IRTM give a larger figure of 184,000 km^2. The region is intermediate in TES thermal inertia, averaging 190–230 mks units. The IRTM rock abundance in this zone was moderate during the Viking era, ranging from 6% to 10%.

[31] Propontis is an area in which local dust storms were frequently seen during southern spring and summer in a systematic survey of MOC WAC images taken during 1999 [*Cantor et al.*, 2001]. Examination of high-resolution NAC images shows that the sharp, narrow tracks left by dust devils were largely absent from Propontis during this season, and only rarely appeared during northern summer. The region is characterized by pronounced albedo variations with distinct but irregular margins. Tapering streaks that arise from topographic obstacles are seldom observed, suggesting that prevailing winds played little part in eroding this region. However, several unusual streaks are seen in MOC image E1103546, centered at 184.98°W, 39.56°N.

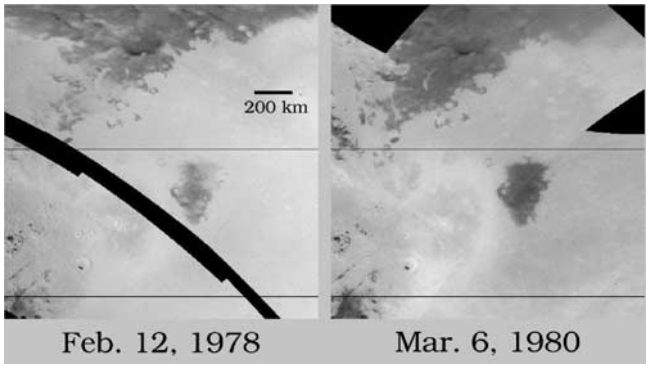

Figure 6. Surface changes at Nilosyrtis and Alcyonius during the Viking era. Two Viking Orbiter views taken on orbits 605A and 347S show changes in albedo patterns already underway. Earlier Mariner 9 observations showed Alcyonius buried, indicating that the surface changes in this region have been going on for at least three decades.

These long, narrow streaks are similar to dust devil tracks but are an order of magnitude wider (~200 m) and several times longer than typical dust devil tracks. They do not show spiral structure or curvilinear planforms and, unlike dust devil tracks, they appear in sets of several subparallel streaks with similar orientations. It is possible that these ephemeral streaks were formed by long-lived, spatially extended gusts in the larger scale dust storms. Such squalls could be produced by fronts in energetic local storms. The peculiar streaks of Propontis may be related to the much larger mesoscale linear streaks found nearby in Amazonis [*Thomas et al.*, 2003], that also form subparallel sets and appear to be produced by local and regional dust storms.

4.6. Southern Tropical Dark Band (Mare Cimmerium–Mare Sirenum)

[32] Mars may have been in an atypical state during the tenure of the Viking Orbiters, in the sense that there was a gap in the dark band that rings the low southern latitudes of the planet. A broad zone centered at 30°S, 180°W was bright as late as 1980 (Viking orbit 323S) but darkened before the arrival of MGS. Nearly 1.8 million km^2 grew visibly darker, reducing the albedo of this region by 21% to 36% to TES values of 0.13 to 0.15. Over the same period, many smaller dark patches were obscured by new dust deposits over the equatorial zone from 10°S–25°S and from 160°W as far as 230°W. The boundary between the newly deposited bright dust and the freshly eroded dark band is relatively abrupt and extends over thousands of kilometers (Figures 2a–2c) but does not correspond to any marked variations in topography or thermal inertia. The changes took place in the southern highlands on a sloping bench that gradually rises from 900 m to 2600 m in elevation. The sharp new albedo boundary does not correspond to the margin of the rugged southern highlands with the smooth northern lowlands, which is several hundred km to the north. Neither is there a distinct change in thermal inertia across the albedo boundary; the TES thermal inertia reduces only slightly from south to north and remains in the range of 210–260 mks units. Interestingly, the albedo boundary appears in the global MOLA laser roughness map [*Neumann et al.*, 2003] as the division between a very rough region to the south (in the low-albedo zone) and an area to the north where the laser returns were saturated, due to either high-amplitude reflections or anomalously long pulse durations indicating high roughness. The simplest explanation is that the saturation is due to the higher albedo of the bright tropical dust; further MOLA analyses may tell whether the region is unusual in surface roughness.

4.7. Southern High-Latitude Band (Mare Chronium–Mare Australis) at Phaethontis

[33] The largest region that altered in appearance is a broad band of the southern highlands that extends southward from about 45°S to 70°S, an area of some 16 million km^2. This appears as a new dark ring around the South Pole in the polar projection of Figure 2c. Both the MOC versus Viking imaging and the TES versus IRTM albedo data show that this region darkened during the past two decades. Imaging data measurements indicate that at least 5.5 million km^2 darkened by 10% or more. TES and IRTM measurements would yield a much larger area darkened (at least 11 million km^2 was affected within the area of mutual TES and IRTM coverage); however, the IRTM measurements do not extend past 60°S. TES albedo in the newly darkened region is 0.13 to 0.15, a change of −0.06 to −0.09 from the IRTM albedo. HST observations [*Bell et al.*, 1999] indicate that the change took place prior to 1995. This change is the most difficult to map, because

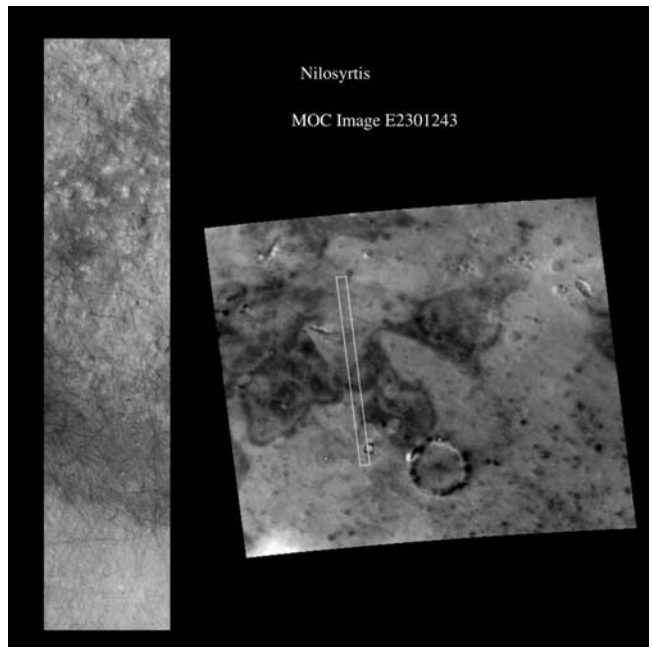

Figure 7. Dust devil tracks in Nilosyrtis. A portion of a MOC NAC image (left) shows a close-up view of recently darkened terrain in western Nilosyrtis at 54.28°N, 292.69°W. The surface in the darkest parts of the picture (near the middle of the footprint plot on the MOC WAC context image, at right) is crisscrossed with filamentary linear streaks that are diagnostic of dust devil tracks. The width of the NAC image is 3.4 km, and the context image is 133 km across. These images were processed by Malin Space Science Systems.

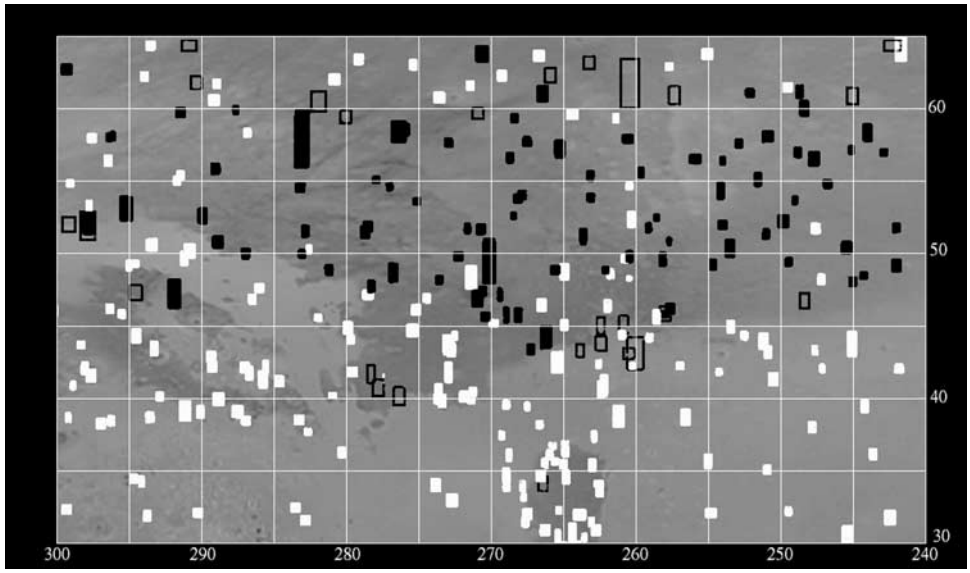

Figure 8. Nilosyrtis dust devil track locations. A survey of MOC NAC images from mission phases AB1 to E06 identified dust devil tracks in 107 NAC images (solid black rectangles). Ambiguous cases, including vague or partially erased tracks, are shown as open rectangles. Definitive nondetections were made in another 180 NAC images (white rectangles). The dust devil tracks are strongly zoned during all seasons, confined to latitudes ~45°N to ~65°N. In areas such as Alcyonius that darkened outside of this latitude band, dust devil tracks are absent and the surface is pervaded instead by linear wind streaks indicative of prevailing winds.

the boundaries of the recently darkened area are diffuse and discontinuous. It was also regarded with some suspicion, since the southernmost images of the Viking color MDIM were data acquired at relatively high phase angles that show albedo variations poorly. Comparison with low-phase-angle Viking images such as those from orbit 507A (phase angle 21 degrees) confirms that some albedo information was lost at these high southern latitudes in the construction of the color MDIM. However, two Viking image sequences that show the area of the southern high-latitude band at low phase angles with good albedo definition verify that the darkening of the band is genuine, at least over certain longitudes. A color sequence taken during orbit 459A shows the region south of Sirenum at 39 degrees phase during southern summer, at Ls 318 degrees. This sequence shows that the latitude band from ~45°S to ~65°S was distinctly brighter than present, at least over longitudes from 190°W to 240°W. Images from orbit 500A at 21 degrees phase suggest that the high-latitude areas from 45°S to 75°S that are presently dark over longitudes from 80°W to 160°W were also bright at this time. Other sequences acquired on orbits 463A and 605A confirm albedo changes over the same longitudes (80°W to 240°W) but in general, low phase coverage of the southern polar region by Viking was sparse.

[34] On the basis of the available low phase angle Viking images, together with the support of the TES and IRTM measurements, we conclude that the darkening of the southern high latitudes between Viking and MGS observations is genuine. All together, the area affected by surface changes in the southern highlands over the past two decades amounts to more than 40 million km^2, nearly a quarter of the surface area of the planet. This figure excludes the known surface changes in the equatorial and northern latitudes of Mars and any activity in dust-covered regions such as Amazonis and Arabia that may have experienced dust deposition and erosion without detectable changes in albedo.

[35] Figure 11 shows an overview of surface changes in Phaethontis Quadrangle, covering a small portion of the new dark ring that appeared across the southern high latitudes and also a sample of changes in the tropical dark band. The bedrock in this region is mostly made up of Plateau Sequence rocks of Hesperian and Noachian age, along with some Hesperian volcanics and ridged plains [*Scott and Tanaka*, 1986]. In the north of the quadrangle, sand dunes and dust devil tracks are absent and the wind streaks indicate that the winds are from the northwest, consistent with GFDL MGCM predictions of light (<5 m/s) northwesterly winds during southern summer. In contrast, most of the wind direction indicators in the middle and southern portions of the quadrangle suggest southeasterly winds, which reach average speeds of ~10 m/s during southern spring according to MGCM predictions. Dust devil tracks are common in southern summer, occasionally reaching very high densities in some locations (e.g., M1301057, E1100101, E1103012). As in Nilosyrtis and Acidalia, the tracks are common in specific latitude bands and rare or absent in others. Figure 12 shows that the tracks found in a cursory survey of MOC NAC images are confined to latitudes from 45°S to 65°S, a range similar to those determined from the northern hemisphere surveys in the Nilosyrtis (section 4.2) and Acidalia (section 4.10) regions.

[36] Much of the area that darkened in the southern half of Phaethontis Quadrangle shows no distinct wind streaks or dust devil tracks at the resolution of the MOC NAC images.

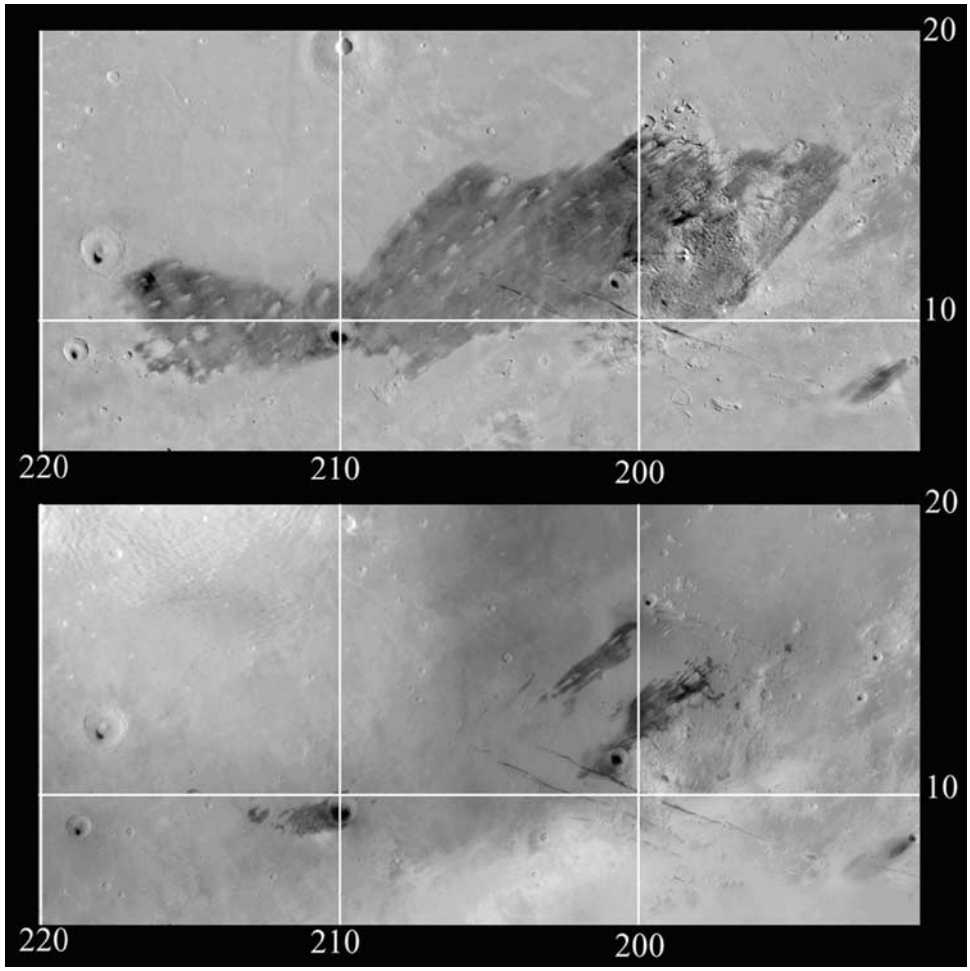

Figure 9. Surface changes at Cerberus. This classical albedo feature largely disappeared during the interval between the (top) Viking and (bottom) MGS observations. The linear bright and dark wind streaks with diffuse albedo boundaries are indicative of erosion by prevailing winds. These images span an east-west distance of 1700 km at 10°N latitude. The MGS mosaic shown is from *Caplinger* [2002].

Instead, diffuse dark bands can be seen extending downwind from "splotch" craters (impact craters occupied by deposits of low-albedo materials). In every case where MOC imaged one of these splotches at high resolution, the images revealed that the low-albedo deposits were dark dunes clustered against the downwind margins of the crater floors (Figure 13). The dunes are located in the northwestern sides of the craters, the northwest walls of the craters appear dark, and diffuse dark bands taper from the craters toward the northwest, consistent with the southeasterly winds predicted by the GFDL MDIM to reach strengths of up to 10 m/s during southern spring. Figure 14 shows the locations of dark dunes identified in the released MOC NAC images of the region. The MOC NAC data set is incomplete, and many of the splotch craters that currently lack coverage by high-resolution images are likely to contain dunes as well. Nevertheless, Figure 14 shows that dunes are ubiquitous throughout the darkened zone. This result likely extends to the rest of the southern high-latitude band, a region of splotches, dunes and related streaks that were described by *Thomas et al.* [1979] and many other papers. Moreover, dark dunes mapped globally from Viking images [e.g., *Ward et al.*, 1985; *Peterfreund*, 1985] and Mars Odyssey THEMIS images (R. Hayward and T. Titus, unpublished data) are distributed throughout the southern high-latitudes where the dark circumpolar ring formed sometime between the Viking era and the present.

4.8. Aonius Sinus

[37] The largest brightening detected by TES took place on Daedalia Planum near the southern end of Tharsis (30°S, 130°W). TES and IRTM albedo measurements suggest that an area of 2.2 million km^2 brightened by at least 10%, whereas the MOC and Viking images give a smaller figure of 1.2 million km^2 visibly affected. The dust deposit formed a new bright gap in the dark band that encircles the planet at southern tropical latitudes. TES albedo in the newly brightened zone ranges from 0.21 up to 0.27. The change took place on the steep terrain of the southern slopes of Tharsis, at elevations from 1400 m to 6200 m above datum. Aonius is another area of moderate to high TES thermal inertia, averaging 165–290 mks units. IRTM rock abundances in this zone were mixed, ranging from 5% to 10% prior to the albedo change.

[38] Lowell Observatory images taken during clear atmospheric conditions show Aonius Sinus bright in 1971 but

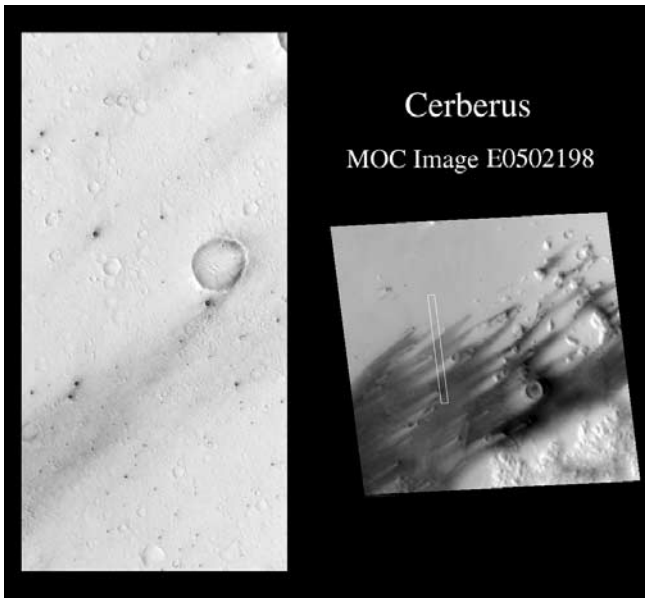

Figure 10. Cerberus close-up. (left) This portion of a MOC NAC image centered at 13.96°N, 199.51°W shows dark-floored craters and incipient erosional streaks that suggest a thin dust cover. The dust within the largest crater is organized into dune-like ripples; elsewhere in Cerberus, such dust-filled craters serve as sources for bright streaks. (right) The context image shows dark erosional streaks that originate at topographic irregularities such as craters and knobs. The width of the NAC image is 3.0 km, and it is excerpted from a point 1/3 of the way from the top of the footprint plot shown in the context image. These images were processed by Malin Space Science Systems.

dark during 1973 [*Martin*, 1974] (note that *Martin et al.* [1992] refer to a darkening of "Claritas"), suggesting that this is another region that alternates between dust-covered and dust-free states over timescales of decades. This episode of brightening apparently took place prior to the Pic du Midi observations of 1988. The eastern side of Aonius darkened again after the global dust storm of 2001.

4.9. Solis Lacus

[39] The classical dark spot Solis Lacus (28°S, 90°W) is among the albedo features most frequently reported to change on Mars, perhaps because it is so easily recognizable as the "eye" of Mars. *Dollfus* [1965, Figure 11] noted changes in this region after the dust storm of 1956. *Lee* [1986] described Viking era changes that took place after the 1977 dust storm. As mentioned in section 3, the region was the site of one of Mars' most recent changes during the dust storm of 2001. MOC images taken prior to the 2001 dust storm show that the entire plateau south of the Valles Marineris (centered at 20°S, 90°W) had darkened relative to its Viking era appearance, affecting an area of 3.1 million km^2. The changes took place within a high plain rimmed by mountain ranges at elevations from 2500 m to 4300 m. The darkening was greatest to the south in Solis Planum (28°S, 90°W) and the east in Thaumasia Planum (20°S, 60°W). TES and IRTM measurements agree with the darkening in the south and east, but do not show darkening to the north in Syria Planum (15°S, 110°W) or Sinai Planum (15°S, 90°W), instead suggesting that brightening took place in these regions. TES albedo is 0.12–0.17 in the darkened zones and 0.18 to 0.25 in bright areas. Thermal inertia over the region averaged 240–340 mks units. Rock abundance here was relatively high in Viking measurements, averaging 6% to 17%.

[40] New dust deposits emplaced during the 2001 dust storm brightened the area to the east of Solis Lacus (Thaumasia Planum), partly restoring the region to its Viking era appearance.

4.10. Acidalia

[41] Several changes took place between Viking and MGS in the neighborhood of the classical low-albedo feature Acidalia. This dark feature enlarged along its margins and a new bright fringe appeared along its eastern edge (30–40°N, 0–15°W). Brightening also occurred across the top of Acidalia along the new north polar bright band seen in Figure 2b. Darkening took place along Acidalia's southern margin (20–30°N, 40–50°W), along with smoothing of the albedo boundary between the dark surfaces to the north and the brighter surfaces to the south. Further darkening developed along both the eastern and western margins, increasing the width of Acidalia across latitude 35°N. There was also extensive darkening of the region to the west of Acidalia, centered at 30°N, 60°W.

[42] MOC images suggest an area of 2.2 million km^2 was affected; however, TES albedo measurements suggest a much larger area of up to 4.6 million km^2 may have altered. TES albedo in the darkened region dropped from ~0.24 to ~0.12. Most of the changes took place on the sloping rim of a basin (Chryse Planitia) where the southern highlands meet the northern plains, at elevations from −4200 m to −1400 m. In common with the other zones of surface change, this is a region of moderate to high TES thermal inertia (average 235–265 mks units), IRTM rock abundance (average 11%–19%), and MOLA roughness.

[43] Aeolian erosion by prevailing winds is chiefly responsible for the surface changes along the southern margin of Acidalia. Figure 15 shows an overview of surface changes in this region, which extend at least 2000 km in the east-west direction. Most of this expanse is occupied by Arcadia Formation volcanics, Amazonian-aged deposits that were subsequently modified by tectonism [*Scott and Tanaka*, 1986]. A cursory survey of high-resolution MOC NAC images detected no dust devil tracks in the recently darkened zone (Figure 16); in common with the Nilosyrtis region, dust devil tracks in Acidalia were found only in higher latitudes ranging from ~50°N to ~65°N. At lower latitudes, where most of the darkening took place, the albedo is controlled by bright and dark linear streaks that taper toward the southwest. Figure 17 shows a close-up view of the newly darkened terrain at 26.10°N, 42.91°W. Most of the dust has been removed from the region already, and the little that remains is concentrated in the sheltered floors of impact craters, where the dust is organized into small dune-like ripples. Bright streaks extend downwind from the dust-filled craters toward the southwest. Much larger dark streaks with the same southwesterly trend can be seen in regional scale images (Figure 15) from both Viking and MGS, and the albedo boundary dividing bright and

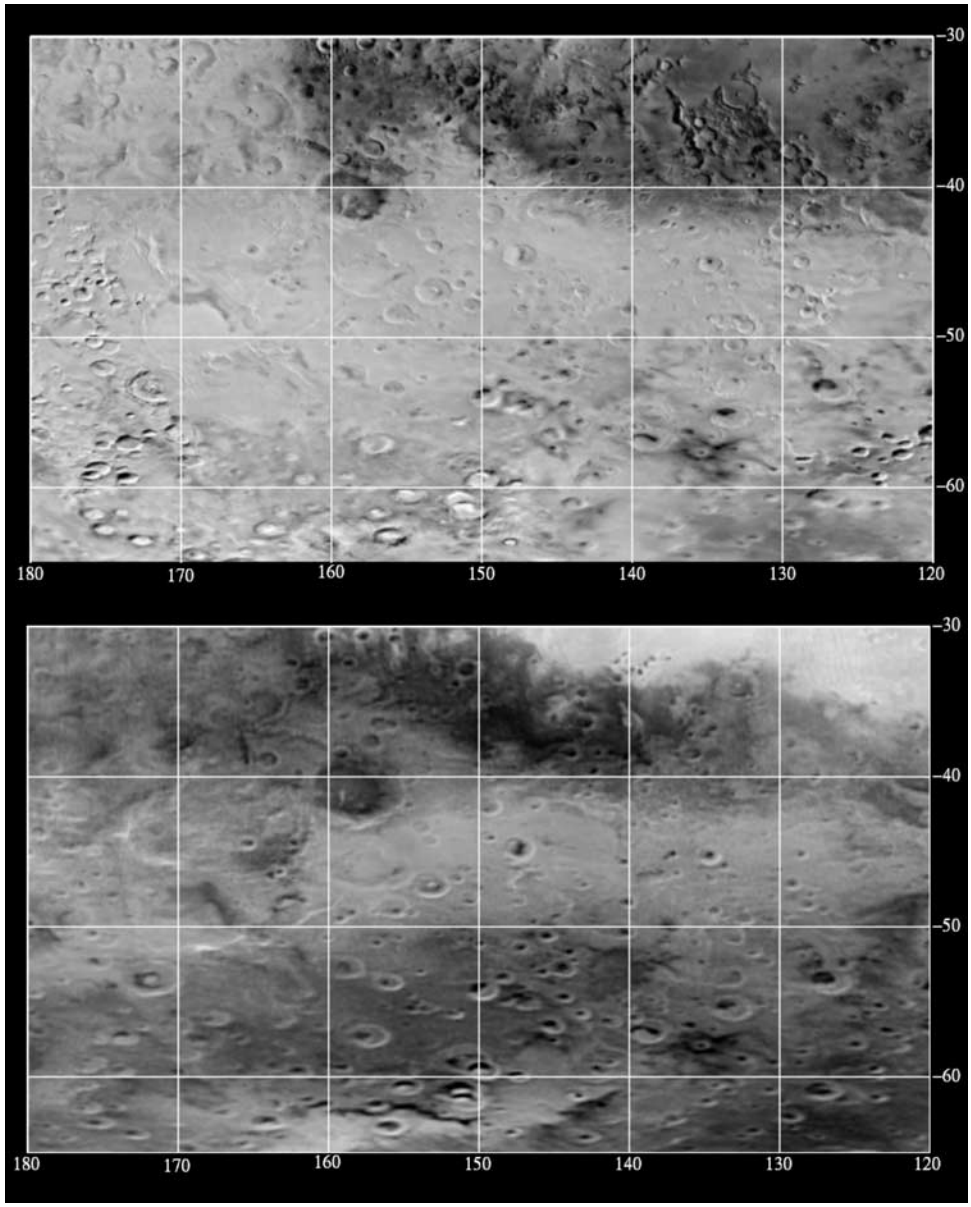

Figure 11. Surface changes in Phaethontis Quadrangle. A broad region with indistinct boundaries south of 50°S darkened between the imaging observations of (top) Viking and (bottom) MGS. This area is part of a large, newly formed dark ring that encircles the south pole. Farther north, both darkening and brightening have taken place at subtropical latitudes from 30°S to 40°S. The images span an east-west distance of 2230 km at 50°S latitude.

dark surfaces can be seen to have advanced in this direction during the interval between Viking and MGS. The GFDL global circulation model predicts calm conditions during southern fall and winter but strong (>10 m/s) northeasterly winds in this region during the southern spring and summer, consistent with the orientation of the wind streaks.

5. Discussion

[44] Some inferences from the global observations can help us begin to interpret the causes of surface changes in general. First, all of the albedo changes discussed above took place in areas of moderate to high thermal inertia (see Table 1 and Figure 4). The MOC versus Viking imaging comparison suggests that a portion of western Amazonis may have also brightened, but this is not borne out by the TES and IRTM albedo measurements (Figure 3). The correlation of surface changes with thermal inertia is consistent with the widely held notion that the changes are caused by deposition and erosion of bright dust that buries and exposes darker bedrock or duricrust. The dust deposits must be thin in comparison to low thermal inertia regions like Amazonis and Arabia, because the thermal inertia of the changeable zones remains high even when they are dust covered (e.g., Cerberus). Second, many of the areas that changed appearance between Viking and MGS have histo-

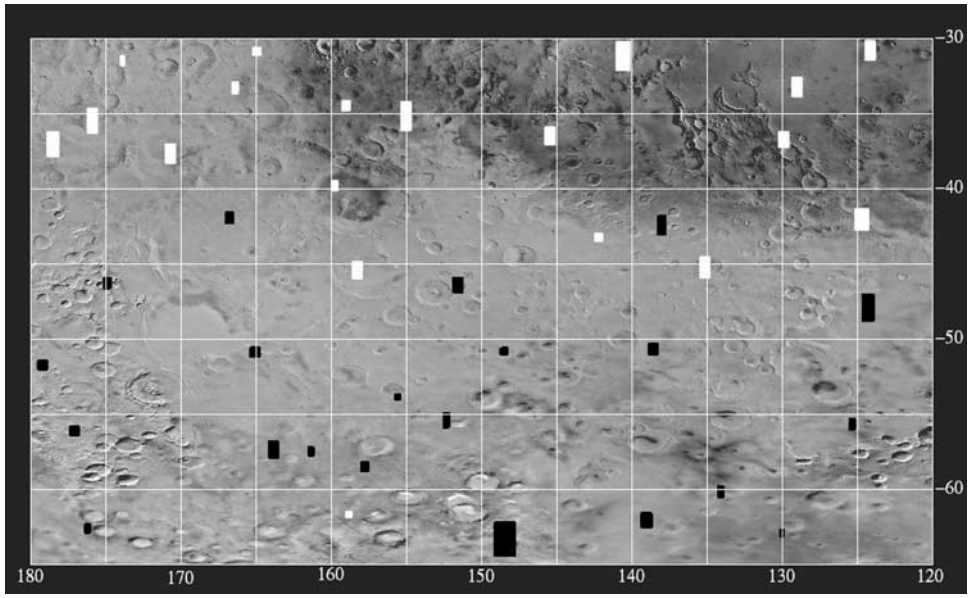

Figure 12. Phaethontis dust devil track locations. The distribution of dust devil tracks in Phaethontis Quadrangle sampled during southern summer is shown superimposed on the Viking image mosaic. Black rectangles indicate the locations of NAC images in which dust devil tracks were observed, whereas white rectangles show the locations of definite nondetections. The size of each rectangle indicates the uncertainty in its location rather than the density of dust devil tracks. This cursory survey suggests that dust devil tracks are concentrated in the mid to high latitudes from 45°S to 65°S.

ries of similar changes in the past, including Syrtis Major, Nilosyrtis, Hyblaeus, Aonius Sinus, and Solis Lacus. Such repeated episodes account for the impression of seasonal surface changes that was long held by many ground-based observers. They also explain how the surface of Mars remains recognizable after a century of telescopic observation, despite the enormous extent of alteration that has taken place between Viking and MGS: according to MOC/Viking imaging estimates, a total area of 56 million km^2 changed albedo by more than 10%, mostly due to darkening in the southern highlands. Alternation of bright, dust-covered periods with darker states during which bedrock is exposed is consistent with the deposition of thin dust layers during global and regional dust storms that are subsequently stripped off by the wind.

[45] But how does this erosion come about? Examination of the surface at higher resolution suggests that several distinct mechanisms may contribute to the aeolian erosion of Mars' surface. Dark sand dunes are scattered throughout the southern high-latitude band and apparently played a role in the darkening of this vast region. Prevailing winds are chiefly responsible for removing dust in low-latitude regions including Acidalia and Cerberus. Local dust storms evidently cause erosion of dust from sites such as Propontis where such activity is frequent. Dust devils evidently strip dust from the northern Nilosyrtis region in sufficient quantities to darken the surface. It is not clear how dust devils accomplish this darkening; although the tracks can significantly reduce albedos over regions in which dust devil track densities are high (up to 50% of the surface is covered by tracks in image E1100101, for example, resulting in a net albedo decrease of at least 15% over the area imaged), the individual dust devil tracks do not seem to persist for more than a few months, on the basis of repeated MOC NAC

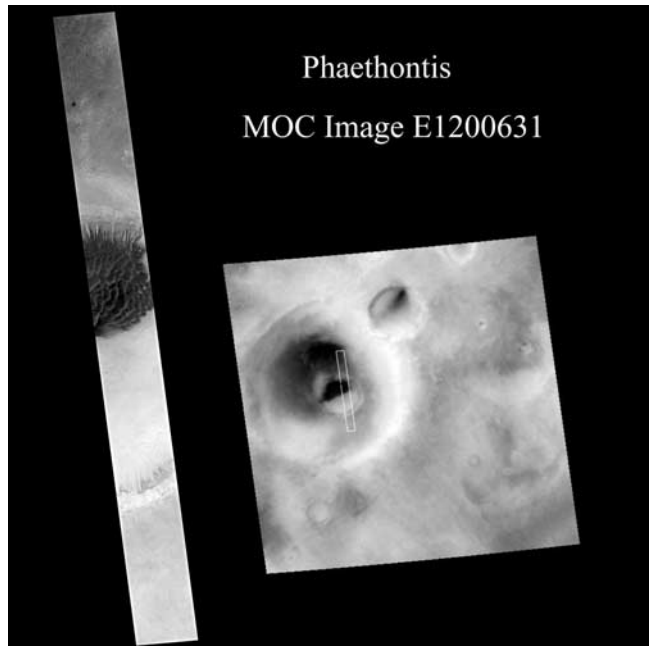

Figure 13. Phaethontis close-up. Many of the dark-floored craters in Phaethontis Quadrangle are occupied by fields of dark dunes that dwarf the bright ripples made by dust. This example is at 52.87°S, 144.42°W. The dune field is huddled to the northwest side of a small crater within a larger crater. Tendrils of sand make their way up gullies on the northwest side of the small crater. The northwest side of the larger exterior crater is blackened, and an outlying dune appears on the exterior crater wall. The MOC NAC image is 3.0 km across. These images were processed by Malin Space Science Systems.

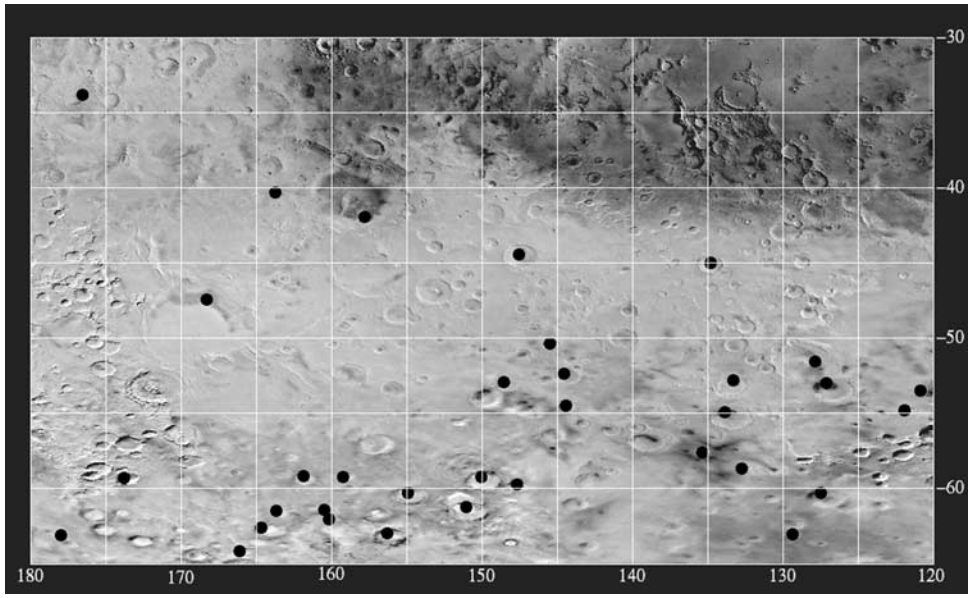

Figure 14. Phaethontis dune locations. The locations of dark dune fields in Phaethontis Quadrangle identified in MOC NAC images up to phase R09 are shown superimposed on the Viking image background. Dark dunes are scattered throughout the area that darkened between Viking and MGS imaging observations. Many of the splotch craters that currently lack high-resolution coverage are likely to contain dunes as well.

imaging of a dozen spots where the tracks can be monitored. Perhaps it is the cumulative diminution of dust in a region where dust devils are active that produces an overall darkening over time, rather than the accumulation of distinct dark tracks on the surface. Alternatively, the dust devils may aggregate the dust locally, redistributing it from a uniform thin layer into concentrated deposits in dunes or in sheltered locations. Other open questions concern the cause and extent of the apparent latitudinal zoning of dust devil tracks. Dust devil tracks in Nilosyrtis, Acidalia and Phaethontis are common during summer seasons at latitudes from ~45 to ~70 degrees, but much rarer at lower latitudes. While dust devils and their tracks have been seen at all Martian latitudes, their contribution to erosion is apparently only significant at mid to high latitudes. *Balme et al.* [2003] carefully quantified dust devil track densities in the great basins of Hellas and Argyre. They noted that dust devil tracks could be found at all latitudes within their study areas (latitudes 15°S to 60°S) but found greater track densities at higher latitudes (from ~45°S to ~60°S in Argyre, and from ~35°S to ~60°S in Hellas; see their Figure 4). The dust devil track distributions in Hellas and Argyre are similar to the qualitative surveys presented here, and support the suggestion of latitudinal control on the frequency of dust devils or the visibility or persistence of their tracks. Further work is needed to clarify the cause of this distribution. For now, we note that the areas in which dust devil tracks accumulate tend to be areas that experience only light summertime winds, according to the numerical model predictions.

[46] The mechanism by which giant sand dunes darken adjacent terrain is another matter of debate. The best studied examples of such albedo changes are in Oxia Palus in western Arabia Terra, where conspicuous dark streaks with bright margins extend southward from numerous dune-filled impact craters. These streaks were noted to have changed in length, albedo, and orientation between observations made by Mariner 6 (1969), Mariner 9 (1972) and Viking 2 (1976–1980) [*Thomas and Veverka*, 1979]. At least three hypotheses have been postulated to explain the albedo changes in Oxia Palus: (a) deposition of fine dark particles eroded from the dunes and carried downwind in suspension; the bright margins would then represent the finest (dust-sized) fraction of the sediment [*Edgett*, 2002]. (b) deposition of coarse sand grains that hopped (via saltation) or rolled (via traction) over the crater rims; the bright margins of the dark streaks could be either dust remobilized by the sand grains [*Thomas et al.*, 1981] or red soil that was disturbed and brightened by the passage of the sand grains [*Mustard*, 1995; *Cooper and Mustard*, 1998]. (c) erosion of bright dust and red soil downwind of the craters by traction and saltation of sand grains escaping from the dunes, revealing a darker substrate; the bright margins of the dark streaks might then represent deposits of dust shed from the eroded zones.

[47] *Edgett* [2002] examined the dark streaks of western Arabia Terra in high-resolution MOC NAC images and found no evidence of morphological differences between the dark streaks and the surrounding untinted surface, ruling out significant deflation in the darkened zones. The images did reveal several small bright streaks arising from dust-filled craters, similar to those seen in recently eroded regions in Cerberus (e.g., MOC image E0301587) and Acidalia (Figure 17). *Edgett* [2002] favored downwind deposition by suspension, on the basis of the absence of dunes on the splotch crater walls and in the dark streaks downwind. On the other hand, erosion of thin coatings of soil or dust in the lee of splotch craters is permitted by the

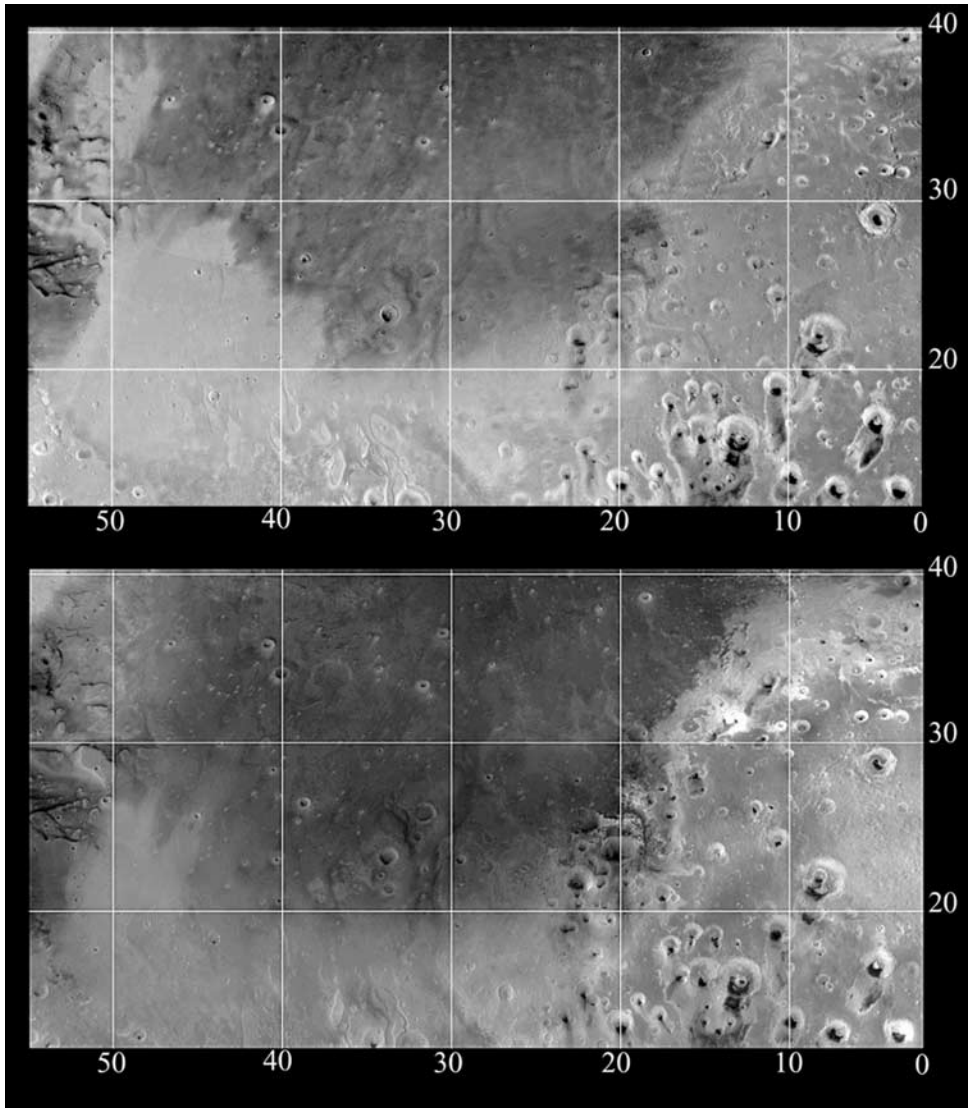

Figure 15. Surface changes in southern Acidalia. The albedo boundary dividing bright and dark surfaces advanced toward the southwest during the interval between (top) Viking and (bottom) MGS imaging observations. Linear wind streaks and diffuse albedo boundaries indicate erosion by prevailing northeasterly winds. These images span an east-west distance of 2700 km at 30°N latitude. The MGS mosaic shown is from *Caplinger* [2002].

observations, as long as the layers removed are much thinner than the scale of topography visible in the MOC NAC images. Such erosion could be produced by the saltation and traction of mobile sand grains originating from the dark dunes, provided that the sand supply is small and does not exceed the removal rate. In either case, the darkening of adjacent surfaces likely takes place when materials are shed from the dark dunes and redeposited downwind.

[48] Martian surface changes reveal the distribution of depositional and erosional zones under present winds and give important clues to the nature of surface materials and the physical processes that alter the appearance of the planet. Only a minimum estimate of the volume of sediment transported by winds on Mars can be obtained from a study of surface albedo changes. Erosion and deposition of dust are likely to be as important in the bright, dust-covered "continents" of Amazonis, Arabia, and Elysium as elsewhere on the planet, yet may produce no significant changes in visible albedo. The details of the surface changes provide constraints on the direction and strength of the winds presently blowing across the Martian surface. The albedo changes affect the distribution of surface heating by insolation, which in turn alters the circulation of the winds that produce the surface changes. Because the most recent changes resulted in darkening of the higher latitudes and general brightening at lower latitudes, these changes would be expected to produce a more uniform overall distribution of surface temperatures if Mars' orbit were circular. However, heating in the southern hemisphere during perihelion surpasses northern hemisphere insolation during aphelion, so the darkening of the southern latitudes may enhance the

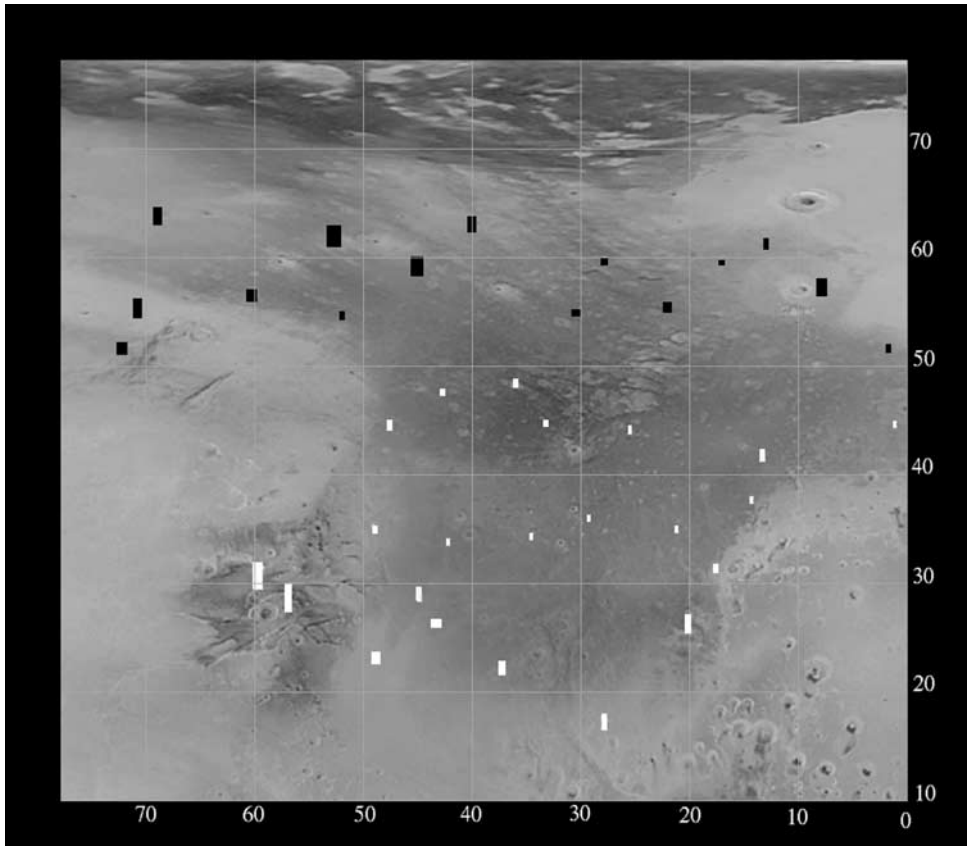

Figure 16. Acidalia dust devil track locations. A cursory survey of northern summertime high-resolution MOC NAC images detected no dust devil tracks along the recently darkened southern margin of Acidalia. In common with the Nilosyrtis region, dust devil tracks in Acidalia were found only in higher latitudes ranging from ~50°N to ~65°N. At lower latitudes, where most of the darkening took place, the albedo is controlled by bright and dark linear streaks that taper toward the southwest.

Hadley circulation and the strong winds and energetic dust storms that typically occur during southern summer.

6. Conclusions

[49] We constructed a cloud-free, summertime mosaic of Mars at it appeared to MGS during the period 1999–2001 and compared it to earlier observations from Viking, Mariner, HST and ground-based telescopes in order to determine how the visible albedo of the planet has altered over time. We quantified the areas affected and examined the topographic setting, thermal inertia, and high-resolution morphology of a few of the surface changes identified in this way. From these considerations we suggest the following interpretations:

[50] 1. Extensive changes in albedo took place during the past three decades of spacecraft exploration of Mars. Up to 1/3 of the surface area of the planet altered in albedo by more than 10% since the Viking era, with the most significant changes in the southern highlands. In general, the Martian surface tended to darken at higher latitudes, particularly in the southern hemisphere, while most of the brightening took place in the equatorial regions. These albedo changes could potentially alter the distribution of surface temperatures due to insolation and the resulting global circulation of winds.

[51] 2. All of the observed surface changes took place in areas of moderate to high thermal inertia and rock abundance, places where bedrock and other coarse-grained material are exposed at the surface and can be buried by dust and exhumed by the wind. This suggests that the changes were caused by deposition of thin dust layers during global and regional dust storms and their subsequent removal by aeolian erosion. It is likely that dust deposition and erosion also take place on thickly mantled, dust-covered regions of low thermal inertial such as Amazonis and Arabia, but this suspected activity does not greatly alter the appearance of the already bright surface.

[52] 3. Preliminary studies of high-resolution images in variable regions suggest that several distinct mechanisms contribute to the erosion of dust on Mars. These processes appear to be globally distributed but tend to be most effective at particular seasons and latitudes. It is likely that further investigation of other Martian surface changes will reveal additional mechanisms of change.

[53] 3.1. Prevailing winds dominate erosion at low latitudes, specifically at Alcyonius, Cerberus, Sirenum, and the southern margin of Acidalia. These winds produce linear bright and dark wind streaks with diffuse margins that typically trend in the direction of strong southern spring and summer winds. Remnant dust in

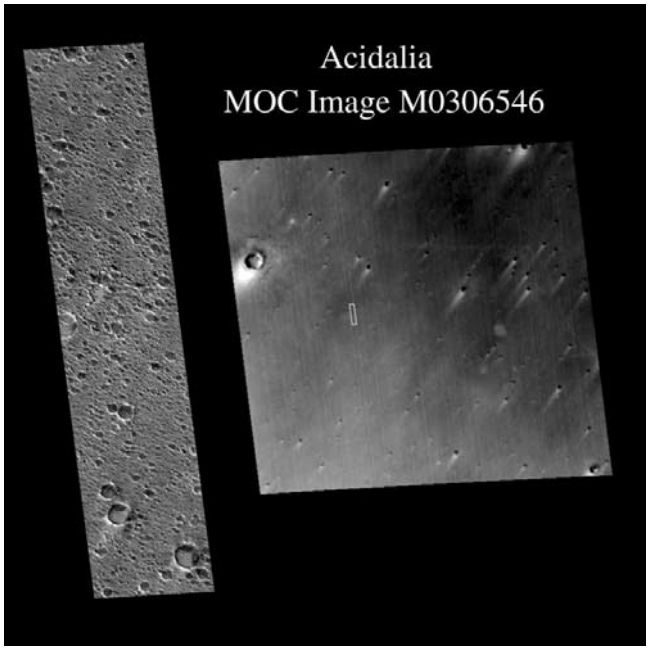

Figure 17. Acidalia close-up. A close-up view of the newly darkened terrain at 26.10°N, 42.91°W shows that most of the bright dust has been removed from the region already. The little dust that remains is concentrated in the sheltered floors of impact craters, where it forms small dune-like ripples. Bright streaks extend toward the southwest, downwind from the dust-filled craters. These images were processed by Malin Space Science Systems.

these regions forms dunelike ripples inside impact craters, trailing bright streaks downwind as it erodes.

[54] 3.2. Dust devils apparently dominate erosion in the high northern latitudes. Recently darkened terrain in Nilosyrtis is crisscrossed by the dark tracks of dust devils, forming irregular albedo boundaries with sharp margins. Some evidence for latitudinal zoning of dust devil tracks is seen in both the northern and southern hemispheres. Dust devil tracks in Nilosyrtis, Acidalia and Phaethontis are common during summer seasons at latitudes from ~45 to ~70 degrees, but much rarer at lower latitudes. Further work is needed to clarify the cause of this distribution.

[55] 3.3. Local dust storms darken areas such as Propontis that exhibit neither dust devil tracks nor consistent wind streaks. Frequent dust storm activity in Propontis results in regional albedo variations with distinct but irregular margins. Ephemeral wind streaks in this area are possibly produced by gusts of wind from seasonal dust storms.

[56] 3.4. Dark sand dunes are concentrated in southern Phaethontis Quadrangle and are widely distributed throughout high southern latitudes, a region that darkened without forming conspicuous albedo boundaries. Erosion of the dunes apparently helped darken the region by staining the surface with dark silt or scouring the region of dust through the saltation and traction of sand particles.

[57] 4. Martian surface changes either occur episodically during global dust storms, or else take place gradually over several years. No evidence was found for seasonal changes in albedo patterns during two Martian years of MGS observations, although surface albedo contrast and obscuration by frosts, clouds and hazes vary periodically on an annual basis. However, many Martian albedo features historically alternate between dust-covered and dust-free states. Surface changes that took place between Viking and MGS in Syrtis Major, Nilosyrtis, Hyblaeus, Aonius Sinus and Solis Lacus reversed earlier changes or were restored to their former appearance during the global dust storm of 2001. On timescales of decades, the surface returns to an average or equilibrium appearance that ensures that the face of Mars remains recognizable in general but different in detail with each passing year.

[58] **Acknowledgments.** Thanks are extended to Alfred McEwen and Conway Leovy for insights into the interpretation of these results and for explaining the nuances of the Viking data processing. Peter Thomas and Stéfane Erard provided thoughtful reviews. Discussions with Tammy Becker, Glenn Bennett, Timothy Titus and many of the scientific and technical staff of the U.S.G.S. Astrogeology Team in Flagstaff contributed to this research. This work was supported by the NASA Mars Data Analysis Program.

References

Akabane, T., K. Iwasaki, Y. Saito, and Y. Narumi (1990), Blue clearing of Syrtis Major at the 1982 opposition, *J. Geophys. Res.*, *95*, 14,649–14,655.

Balme, M. R., P. L. Whelley, and R. Greeley (2003), Mars: Dust devil track survey in Argyre Planitia and Hellas Basin, *J. Geophys. Res.*, *108*(E8), 5086, doi:10.1029/2003JE002096.

Bell, J. F., M. J. Wolff, T. C. Daley, D. Crisp, P. B. James, S. W. Lee, J. T. Trauger, and R. W. Evans (1999), Near-infrared imaging of Mars from HST: Surface reflectance, photometric properties, and implications for MOLA data, *Icarus*, *138*, 25–35.

Berman, D. C., and W. K. Hartmann (2002), Recent fluvial, volcanic, and tectonic activity on the Cerberus Plains of Mars, *Icarus*, *159*, 1–17.

Burr, D. M., A. S. McEwen, and S. E. H. Sakimoto (2002a), Recent aqueous floods from the Cerberus Fossae, Mars, *Geophys. Res. Lett.*, *29*(1), 1013, doi:10.1029/2001GL013345.

Burr, D. M., J. A. Grier, A. S. McEwen, and L. P. Keszthelyi (2002b), Repeated aqueous flooding from the Cerberus Fossae: Evidence for very recently extant, deep groundwater on Mars, *Icarus*, *159*, 53–73.

Cantor, B. A., P. B. James, M. Caplinger, and M. J. Wolff (2001), Martian dust storms: 1999 Mars Orbiter Camera observations, *J. Geophys. Res.*, *106*, 23,653–23,688.

Capen, C. F. (1976), Martian albedo feature variations with season: Data of 1971 and 1973, *Icarus*, *28*, 213–230.

Caplinger, M. A. (2002), Mars Orbiter Camera global mosaic, *Proc. Lunar Planet. Sci. Conf. 33rd*, abstract 1405.

Chaikin, A. L., T. A. Maxwell, and F. El-Baz (1981), Temporal changes in the Cerberus region of Mars—Mariner 9 and Viking comparisons, *Icarus*, *45*, 167–178.

Christensen, P. R. (1986), The spatial distribution of rocks on Mars, *Icarus*, *68*, 217–238.

Christensen, P. R. (1988), Global albedo variations on Mars: Implications for active aeolian transport, deposition, and erosion, *J. Geophys. Res.*, *93*, 7611–7624.

Christensen, P. R., et al. (2001), Mars Global Surveyor Thermal Emission Spectrometer experiment: Investigation description and surface science results, *J. Geophys. Res.*, *106*, 23,823–23,872.

Cooper, C. D., and J. F. Mustard (1998), Rates of erosion in Oxia Palus, Mars, *Proc. Lunar Planet. Sci. Conf. 29th*, abstract 1164.

de Vaucouleurs, G. H. (1954), *Physics of the Planet Mars: An Introduction to Areophysics*, Faber and Faber, London.

Deal, K. S., R. E. Arvidson, and G. A. Neumann (2003), The surface roughness of terrains on Mars, in *Sixth International Conference on Mars*, abstract 3170, Lunar and Planet. Inst., Houston, Tex.

Dollfus, A. (1965), Etude de la planete Mars de 1954–1958, *Ann. Astrophys.*, *28*, 722–754.

Edgett, K. S. (2002), Low-albedo surfaces and eolian sediment: Mars Orbiter Camera views of western Arabia Terra craters and wind streaks, *J. Geophys. Res.*, *107*(E6), 5038, doi:10.1029/2001JE001587.

Edgett, K. S., and M. C. Malin (2000), Martian dust raising and surface albedo controls: Thin, dark (and sometimes bright) streaks and dust devils

in MGS MOC high resolution images, *Proc. Lunar Planet. Sci. Conf. 31st*, abstract 1073.
Edmonds, J. L., and M. S. Robinson (2003), New Mariner 6 and 7 mosaics of Mars: Clues about time variable surface features, *Proc. Lunar Planet. Sci. Conf. 34th*, abstract 1436.
Erard, S. (2000), The 1994–1995 apparition of Mars observed from Pic-du-Midi, *Planetary Space Sci.*, *48*, 1271–1287.
Erard, S., J.-P. Bibring, O. Forni, J. Mustard, and J. W. Head (1991), Spatial variations in composition of the Valles Marineris and Isidis Planitia regions of Mars derived from ISM data, *Proc. Lunar Planet. Sci. Conf. 21st*, 437–455.
Fenton, L. K. (2003), Aeolian processes on Mars: Atmospheric modeling and GIS analysis, Ph.D. thesis, Calif. Inst. of Technol., Pasadena.
Grant, J. A., and P. H. Schultz (1987), Possible tornado-like tracks on Mars, *Science*, *237*, 883–885.
Greeley, R., and J. Guest (1987), Geologic map of the eastern equatorial region of Mars, *U.S. Geol. Surv. Misc. Invest. Ser., Map I-1802-B*.
Kieffer, H. H., P. A. Davis, and L. A. Soderblom (1982), Mars' global properties—Maps and applications, *Proc. Lunar Planet. Sci. Conf. 12th*, 1395–1417.
Lecacheux, J., P. Drossart, C. Buil, P. Laques, E. Thouvenot, and P. Guerin (1991), CCD images of Mars with the 1 M reflector atop Pic-du-Midi, *Planet. Space Sci.*, *39*, 273–279.
Lee, S. W. (1986), Regional sources and sinks of dust on Mars: Viking observations of Cerberus, Solis Planum, and Syrtis Major, in *Symposium on Mars: Evolution of Its Climate and Atmosphere, LPI Contrib. 599*, p. 57, Lunar and Planet. Inst., Houston, Tex.
Lee, S. W., M. J. Wolff, P. B. James, R. T. Clancy, J. F. Bell, and L. J. Martin (1996), HST observations of Mars: Time-variable albedo in the Cerberus region, *Bull. Am. Astron. Soc.*, *28*, 1061.
Malin, M. C., and K. S. Edgett (2001), Mars Global Surveyor Mars Orbiter Camera: Interplanetary cruise through primary mission, *J. Geophys. Res.*, 23,429–23,570.
Martin, L. J. (1974), The major Martian dust storms of 1971 and 1973, *Icarus*, *23*, 108–115.
Martin, L., P. B. James, A. Dollfus, K. Iwasaki, and J. D. Beish (1992), Telescopic observations: Visual, photographic, polarimetric, in *Mars*, edited by H. H. Kieffer et al., pp. 34–70, Univ. of Ariz. Press, Tucson.
McEwen, A. S., L. A. Soderblom, T. L. Becker, E. M. Lee, J. D. Swann, R. Aeschliman, and R. M. Batson (1994), Global color views of Mars (abstract), *Proc. Lunar Planet. Sci. Conf. 25th*, 871–872.
Mellon, M. T. (1997), Small-scale polygonal features on Mars: Seasonal thermal contraction cracks in permafrost, *J. Geophys. Res.*, *102*, 25,617–25,628.
Mellon, M. T., K. A. Kretke, M. D. Smith, and S. M. Pelkey (2002), A global map of thermal inertia from Mars Global Surveyor mapping-mission data, *Proc. Lunar Planet. Sci. Conf. 33rd*, abstract 1416.
Moersch, J. E. (1998), Telescopically-derived constraints on the composition and thermophysical properties of the Martian surface, Ph.D. thesis, Cornell Univ., Ithaca, N. Y.
Moersch, J., J. Bell, L. Carter, T. Hayward, P. Nicholson, S. Squyres, and J. van Cleve (1997), What happened to Cerberus? Telescopically observed thermophysical properties of the Martian surface, paper presented at Mars Telescopic Observations Workshop II, Univ. of Ariz., Tucson.
Mustard, J. F. (1995), Are dark red soils and bright dust on Mars related through mineralogic phase changes?, *Proc. Lunar Planet. Sci. Conf. 26th*, abstract 1021.
Neumann, G. A., J. B. Abshire, O. Aharonson, J. B. Garvin, X. Sun, and M. T. Zuber (2003), Mars Orbiter Laser Altimeter pulse width measurements and footprint-scale roughness, *Geophys. Res. Lett.*, *30*(11), 1561, doi:10.1029/2003GL017048.
Peterfreund, A. R. (1985), Contemporary aeolian processes on Mars: Local dust storms, Ph.D. thesis, Ariz. State Univ., Phoenix.
Plescia, J. B. (1990), Recent flood lavas in the Elysium region of Mars, *Icarus*, *88*, 465–490.
Plescia, J. B. (2003), Cerberus Fossae, Elysium, Mars: A source for lava and water, *Icarus*, *164*, 79–95.
Pleskot, L. K., and E. D. Miner (1981), Time variability of Martian bolometric albedo, *Icarus*, *45*, 179–201.
Sagan, C., J. Veverka, P. Fox, R. Dubisch, J. Lederberg, E. Levinthal, L. Quam, R. Tucker, J. B. Pollack, and B. A. Smith (1972), Variable features on Mars: Preliminary Mariner 9 television results, *Icarus*, *17*, 346–372.
Sagan, C., et al. (1973), Variable features on Mars: 2. Mariner 9 global results, *J. Geophys. Res.*, *78*, 4163–4196.
Scott, D., and K. Tanaka (1986), Geologic map of the western equatorial region of Mars, *U.S. Geol. Surv. Misc. Invest. Ser., Map I-1802-A*.
Seibert, N. M., and J. S. Kargel (2001), Small-scale Martian polygonal terrain: Implications for liquid surface water, *Geophys. Res. Lett.*, *28*, 899–902.
Slipher, E. C. (1962), A photographic history of Mars, 1905–1961, Lowell Observ., Flagstaff, Ariz.
Slipher, E. C. (1964), A photographic study of the brighter planets, Lowell Observ., Flagstaff, Ariz.
Smith, D., G. Neumann, R. E. Arvidson, E. A. Guinness, and S. Slavney (2003), Mars Global Surveyor Laser Altimeter Mission Experiment Gridded Data Record, *MGS-M-MOLA-5-MEGDR-L3-V1.0*, NASA Planet. Data Syst., Washington, D. C.
Soderblom, L. A., K. Edwards, E. M. Eliason, E. M. Sanchez, and M. P. Charette (1978), Global color variations on the Martian surface, *Icarus*, *34*, 446–464.
Thomas, P., and J. Veverka (1979), Seasonal and secular variation of wind streaks on Mars: An analysis of Mariner 9 and Viking data, *J. Geophys. Res.*, *84*, 8131–8146.
Thomas, P., J. Veverka, and R. Campos-Marquetti (1979), Frost streaks in the south polar cap of Mars, *J. Geophys. Res.*, *84*, 4621–4633.
Thomas, P., J. Veverka, S. Lee, and A. Bloom (1981), Classification of wind streaks on Mars, *Icarus*, *45*, 124–153.
Thomas, P. C., P. Gierasch, R. Sullivan, D. S. Miller, E. Alvarez del Castillo, B. Cantor, and M. T. Mellon (2003), Mesoscale linear streaks on Mars: Environments of dust entrainment, *Icarus*, *162*, 242–258.
Veverka, J. (1975), Variable features on Mars V: Evidence for crater streaks produced by wind erosion, *Icarus*, *25*, 595–601.
Veverka, J. (1976), Variable features on Mars. VII: Dark filamentary markings on Mars, *Icarus*, *27*, 495–502.
Veverka, J., C. Sagan, L. Quam, R. Tucker, and B. Eross (1974), Variable features on Mars III: Comparison of Mariner 1969 and Mariner 1971 photography, *Icarus*, *21*, 317–368.
Veverka, J., C. Sagan, and R. Greeley (1976), Variable features on Mars. VI: An unusual crater streak in Mesogaea, *Icarus*, *27*, 241–253.
Veverka, J., P. Thomas, and R. Greeley (1977), A study of variable features on Mars during the Viking primary mission, *J. Geophys. Res.*, *82*, 4167–4187.
Ward, A. W., K. B. Doyle, P. J. Helm, M. K. Weisman, and N. E. Witbeck (1985), Global map of eolian features on Mars, *J. Geophys. Res.*, *90*, 2038–2056.
Wilson, R. J., and K. Hamilton (1996), Comprehensive model simulation of thermal tides in the Martian atmosphere, *J. Atmos. Sci.*, *53*, 1290–1326.

P. E. Geissler, U.S. Geological Survey, 2255 North Gemini Drive, Flagstaff, AZ 86001, USA. (pgeissler@usgs.gov)